

## 1 Protein film electrochemistry

2 Julea N. Butt<sup>1†</sup>, Lars J. C. Jeuken<sup>2†</sup>, Huijie Zhang<sup>2</sup>, Joshua A. J. Burton<sup>1</sup>, Alexander L. Sutton-Cook<sup>1</sup>

3 <sup>1</sup>School of Chemistry and School of Biological Sciences, University of East Anglia, Norwich Research  
4 Park, Norwich, NR4 7TJ, U.K.

5 <sup>2</sup>Leiden Institute of Chemistry, Leiden University, PO box 9502, Leiden 2300 RA, The Netherlands

6 †e-mail: [j.butt@uea.ac.uk](mailto:j.butt@uea.ac.uk), [l.j.c.jeuken@lic.leidenuniv.nl](mailto:l.j.c.jeuken@lic.leidenuniv.nl)

7  
8 **ABSTRACT:** Protein Film Electrochemistry (PFE) is a powerful suite of electroanalytical techniques used  
9 to investigate the properties of redox proteins. The proteins under investigation are adsorbed as a  
10 (sub-)monolayer film on an electrode surface. Direct electron transfer between the immobilized  
11 protein and working electrode gives rise to an electrical current that visualizes and quantifies redox  
12 processes occurring within the protein. Advantages of PFE include low sample requirements —  
13 typically less than a nanomole protein — high sensitivity and the ability to resolve redox chemistry in  
14 the electrochemical potential and time domains. This Primer provides a guide to using PFE for  
15 quantitative thermodynamic and kinetic descriptions of half-reactions (redox reactions) and coupled  
16 chemical processes, including ligand binding, ligand unbinding and redox catalysis. Applications of PFE  
17 in developing biosensors, facilitating energy conversion and resolving enzyme mechanisms are  
18 highlighted. Finally, the state-of-the-art and prospects for novel experimental and theoretical  
19 approaches are discussed.

## 21 INTRODUCTION

22 Redox proteins are ubiquitous in biology. They perform electron transfer reactions and redox catalysis  
23 that are essential to life, for example, in photosynthesis and respiration. These functions are enabled  
24 by redox active cofactors, one or more per protein, including copper, molybdenum, heme, non-heme  
25 iron and flavin<sup>1,2</sup>. During physiologically relevant electron exchange the redox cofactors are positioned  
26 within 14 Å of one another<sup>3</sup>. Electron transfer between proteins is supported by cofactors near the  
27 protein surface. By contrast, redox catalysis may occur adjacent to cofactors buried deep within a  
28 peptide matrix. This allows redox transformation of the substrate in a site shielded from solvent,  
29 avoiding non-productive and possibly toxic redox reactions. Additional redox cofactors positioned as  
30 a chain enable electrons to be relayed between the active site and protein surface, **FIG. 1A**.

31 Protein film electrochemistry (PFE) — also termed protein film voltammetry (PFV) and protein  
32 monolayer electrochemistry — is a powerful tool for investigating the properties of redox proteins<sup>4-  
33 11</sup>. PFE studies protein electron transfer and redox catalysis using dynamic electrochemistry applied to  
34 a (sub-)monolayer film of redox active protein immobilised on the surface of a working electrode (WE).  
35 As shown schematically in **FIG. 1A**, there is direct electron exchange between the immobilised protein  
36 and WE, which gives rise to an electric current. The produced current visualises and quantifies redox  
37 processes within the protein. Using this approach, quantitative thermodynamic and kinetic  
38 descriptions of half-reactions (redox reactions) and coupled chemical processes, including redox  
39 catalysis, can be readily obtained. These descriptions result from considering direct electron transfer  
40 between the WE and adsorbed protein, **FIG. 1A**. PFE is different to experiments that use mediated  
41 electron transfer, where an additional redox-active species, often called a mediator, is introduced to  
42 shuttle electrons between the protein and WE.

43 PFE traces its roots back to the 1990s, when electrochemistry of adsorbed proteins was reported<sup>12 13</sup>  
44 <sup>14</sup> that agreed with the properties defined by established biochemical assays of proteins in solution<sup>6</sup>.  
45 The adsorbed proteins retained functional integrity and the electrode-protein interactions could be  
46 considered to mimic those between the protein of interest and its biological redox partner. Today the  
47 advantages of PFE for revealing and understanding redox protein activity are widely recognised. The  
48 equipment is extremely low cost compared to modern biophysical methods and spectroscopies, with  
49 lower protein requirements, often sub-picomole in an adsorbed film prepared from a solution of less  
50 than a nanomole protein. The protein-coated electrode often survives changes in the solution to  
51 which it is immersed, meaning the impact of varying conditions can be readily assessed. Signals are  
52 sharp and high-resolution, enabling complex behaviour to be controlled, dissected, and elucidated  
53 because there are no contributions from relatively slow protein diffusion. In a single experiment, the  
54 current is measured across a wide, continuous potential range for the desired time — from under a  
55 second to several hours — allowing many different and defined changes to be made to the  
56 composition, pH and temperature of the immersion solution.

57 This Primer will describe the equipment typically used for PFE and provide the practical and theoretical  
58 background needed to perform and interpret electrochemical experiments. The article focuses on  
59 explaining how standard concepts available in electrochemistry<sup>15,16</sup> and biochemistry<sup>17</sup> textbooks  
60 typically apply to PFE, illustrating how PFE describes redox couples, ligand binding and redox catalysis.  
61 Detailed discussions are kept to the simplest scenarios. However, more complex behaviours are  
62 touched upon, with references to works that illustrate how those results may be investigated and  
63 explained.

64 In this Primer, cyclic voltammetry (CV) and chronoamperometry (CA) will be focused on, as they are  
65 widely used and provide the most immediately intuitive and quantitative descriptions of protein redox  
66 chemistry. In CV, the WE potential is swept back and forth across a region of interest at a specified  
67 scan rate, **FIG. 1B**. The resulting current is measured simultaneously and reported as a cyclic  
68 voltammogram that plots current versus WE potential. In CA, the potential of the WE is stepped  
69 instantaneously between defined values at specified time points, **FIG. 1C**. The resulting current is  
70 reported versus time in an amperograms. Conditions can be changed as desired, for instance, a  
71 reactant can be introduced in both types of experiment.

72 It is important to recognise that the current in both CV and CA has two components that are  
73 superimposed<sup>15</sup>. The Faradaic current is due to electron transfer between the electrode and redox  
74 active proteins in the (sub-)monolayer film, **FIG. 1A** (red arrows). Non-Faradaic current (capacitance)  
75 is due to charging and discharging of the electrode–solution interface and electrons are not  
76 transferred across that interface, **FIG. 1A** (brown arrows). PFE is interested in the Faradaic current, as  
77 it reports the redox chemistry of the protein. Care must be taken to accurately extract the Faradaic  
78 current from the measured current. By convention, Faradaic current is negative during net reduction  
79 and positive for net oxidation.

80

## 81 **EXPERIMENTATION**

82 The equipment needed for PFE depends on the desired application, but requires at least a  
83 potentiostat<sup>18</sup>, an electrochemical cell and analytical software. The electrochemical cell contains a  
84 counter electrode (CE) and reference electrode (RE) in addition to the WE. During measurements the  
85 WE may be stationary or rotating. The latter is particularly useful when studying redox catalysis and a  
86 rotating disk electrode (RDE)<sup>15</sup> allows controlled substrate delivery to the adsorbed enzyme. These

87 experiments can be extended to use a rotating ring disk electrode (RRDE)<sup>15</sup>, which forces the products  
88 of enzyme catalysis to flow across a second WE — a concentric ring around the central enzyme coated  
89 disk electrode — for analysis by amperometry.

### 90 **Potentiostats and working electrode rotators**

91 Potentiostats can be purchased from many manufacturers. Alternatively, the instrument can be made  
92 in-house<sup>19</sup> for a fraction of the cost. The ideal instrument will depend on the specific requirements  
93 and funds available. All potentiostats can perform basic CV and CA methods. The specifications that  
94 require special attention for PFE are current range; scan rate or band width range; capacity for  $iR$   
95 compensation, where  $I$  is current and  $R$  is resistance; ability to use RRDEs; and ability to perform  
96 analogue CV by applying a true linear voltage ramp to the WE, **FIG. 1B**, in addition to CV, which  
97 approximates the linear ramp with a staircase waveform, and is the primary CV method in  
98 contemporary potentiostats<sup>18</sup>.

99 PFE typically uses WEs with a surface area of  $< 1 \text{ cm}^2$ , scan rates in CV  $< 100 \text{ V/s}$  and potential steps in  
100 CA of  $< 1 \text{ V}$ . Under these conditions, currents are in the nA to mA range, which is adequately covered  
101 by all commercial potentiostats. However, if the intended applications are in bioelectrocatalysis with  
102 WEs that have larger surface areas, higher current ranges might be required.

103 When studying the kinetics of electron transfer or coupled reactions, fast-scan CV (scan rate  $>100$   
104 mV/s) is a powerful tool<sup>6,20-22</sup>. As a result, the scan rate capabilities of the potentiostat should be  
105 considered. The area under a redox peak, the non-catalytic CV, can deviate from theory when using  
106 staircase CV<sup>23</sup>, which is the standard method in most contemporary potentiostats<sup>18</sup>. If the protein  
107 coverage analysis needs to be accurate or when studying reaction kinetics, potentiostats that can  
108 measure analog CV should be considered.

109 For both non-catalytic fast scan and catalytic PFE, currents in the high  $\mu\text{A}$  to mA range can be obtained.  
110 This can lead to significant potential drops due to solution resistance<sup>24</sup>. As current flows through the  
111 electrochemical cell, a potential difference is required across the electrolyte solution to drive ion  
112 mobility and overcome solution resistance. As a result, the potential at the WE interface has a lower  
113 magnitude than the potential applied by the potentiostat. For instance, if the solution resistance is  
114  $100 \Omega$ , a current of  $100 \mu\text{A}$  leads to a potential shift of  $10 \text{ mV}$  ( $V = iR$ , where  $V$  is potential). Potential  
115 drop can be reduced by minimizing the solution resistance, but can also be compensated for by  
116 potentiostats with  $iR$  compensation capabilities<sup>24</sup>.

117 The sensitivity of potentiostats to electronic noise<sup>18</sup> is an important property. However, this property  
118 cannot be determined from specifications and can only be established by trying different potentiostats  
119 under laboratory conditions. Where possible, the electrochemical cell should be placed in a Faraday  
120 cage to reduce electronic noise. Suitable Faraday cages are readily constructed from commercially  
121 sourced electrical boxes, typically steel, with holes for the electrical leads. Alternatively, Faraday cages  
122 can be made from a wire mesh, which enables the electrochemical cell to be observed during  
123 measurements, plus easy access for electrical leads and other connections, such as gas lines.

124 Rotators for use with RDEs are available from several suppliers. Differences include the ability to use  
125 RRDEs, an integrated enclosure for the rotator shaft, variable distances between the controller and  
126 rotator shaft, and the range of electrodes and electrochemical cells compatible with the rotator. The  
127 choice of instrument will be influenced by the ring and disk electrode materials, and whether the  
128 electrochemical cell needs to be serviced by gas supply lines or temperature-controlled water.  
129 Anaerobic experiments also need to consider how readily the rotator can be positioned and operated  
130 within a nitrogen-filled chamber.

### 131 **Electrochemical cells, CE and RE**

132 There are many manufacturers of electrochemical cells, cEs and rEs. For many PFE applications, a  
133 tailor-made electrochemical cell is worth considering, but requires access to a glass blower or fine-  
134 mechanical facility. The wide range of PFE applications means there is no single best cell design.  
135 Variables to consider include the distance between the RE and WE, the need for a RDE or RRDE, and  
136 auxiliary methods, such as illumination for photo-electrochemistry<sup>25,26</sup> or combination with  
137 microscopy or spectroscopy<sup>27</sup>. In **FIG. 2**, several example cell designs are provided with a short  
138 explanation of their properties and specific applications.

139 Alongside the cell, the three electrodes — or four electrodes for a RRDE — are key to PFE. The CE  
140 ensures electroneutrality of the electrolyte solution. For every Faradaic electron transfer at the WE,  
141 an opposite electron transfer is required at the CE. In PFE, the CE is almost always platinum.  
142 Electrochemical currents in PFE are typically low mA or less, meaning a small platinum wire (< 2 cm)  
143 is sufficient. The most used and convenient RE is Ag/AgCl (saturated KCl) although others can be used.  
144 Trace amounts of chloride ions, which leak out of the RE into the electrolyte, can affect the results for  
145 some applications. In this case, a double junction RE is advised, where the Ag/AgCl RE is placed inside  
146 a jacket. This can be achieved by sourcing a double-junction RE or by designing an electrochemical cell  
147 with a double junction, **FIG. 2B,C**. Drift from the quoted potential<sup>15</sup> can occur if the RE is not  
148 maintained. rEs are easily calibrated by comparing the open cell potential with respect to a trusted  
149 RE. If a trusted RE is not available, the CV of a redox couple with known reduction potential — such as  
150 ferri/ferrocyanide — can be measured under controlled temperature, pH and ionic strength.  
151 Potentials measured versus a Ag/AgCl (saturated KCl) RE at 25°C are typically converted to values  
152 versus the standard hydrogen electrode (SHE) by adding +0.197 V<sup>15</sup>.

153

### 154 **Working electrodes**

155 In PFE, the most important electrode is the WE. To form an electroactive protein film, the redox  
156 protein needs to be immobilised on the WE while retaining its native tertiary and quaternary structure  
157 and activity. Proteins can be physisorbed or chemisorbed on the electrode surface, with physisorption  
158 being the most common<sup>28</sup>. Many proteins are adsorbed via electrostatic interactions, although rarer  
159 hydrophobic interactions are known. Electrostatic interaction and protein immobilisation are affected  
160 by the ionic strength and pH of the electrolyte, as the pH determines the charge on the protein surface.  
161 Electrolyte solutions in PFE are always pH buffered. To control the potential drop across the WE  
162 without disrupting the electrostatic interaction between the protein and WE, an ionic strength of ~0.1  
163 M is often a good compromise. Adsorption/desorption is an entropic process, making temperature an  
164 important variable. Lower temperatures improve the film stability but lower catalytic rates.  
165 Chemisorption can be achieved by reacting an amino acid side chain group with the electrode surface<sup>29</sup>  
166 or by affinity interaction<sup>30</sup>. Chemisorbing proteins is more time-consuming than physisorption but can  
167 lead to more stable protein films<sup>31</sup>.

168 Electron transfer rates decrease exponentially with distance between the donor and acceptor.  
169 Suitable electron transfer kinetics (< ms) for PFE requires the distance between at least one redox  
170 cofactor and the electrode surface to be less than 2 nm. In practice this means that the protein needs  
171 to orient correctly upon adsorption, **FIG. 1A**. One approach is to use a heterogeneous electrode  
172 surface, in terms of both geometric structure and surface chemistry. Heterogeneity increases the  
173 possibility that some immobilised proteins are correctly orientated, even if most are electrochemically  
174 silent.

175 Three widely used WE materials are pyrolytic graphite edge (PGE) plane, modified gold and indium-  
176 tin oxide (ITO), although others have successfully been used. The surface of PGE electrodes exposes  
177 the side edges of the graphene sheets, enabling the carbon interface to form a rough surface with  
178 multiple carbon oxide chemistries. PGE electrodes are quickly and easily cleaned by polishing the  
179 surface with an aqueous slurry of alumina or diamond powder, typically 1-micron particles, followed  
180 by a brief treatment in a water-bath sonicator to remove particles. This quick preparation means PGE  
181 electrodes are a convenient experimental tool. The PGE surface is negatively charged due to presence  
182 of carboxylic acids. Consequently, co-adsorbates are required for redox proteins that are negatively  
183 charged or have a negative surface charge close the co-factor orientated towards the electrode  
184 surface. Good co-adsorbates are polylysine, neomycin or polymyxin B, which are added to the  
185 electrolyte or protein solution before they are applied to the electrode. The surface of PGE and other  
186 graphite electrodes can also be controlled by adsorption of polycyclic aromatic hydrocarbon  
187 derivatives, such as pyrene derivatives, which form stable pi-stacking interactions<sup>32</sup>. Alternatively, PGE  
188 can be chemically modified to alter its surface chemistry by electrografting. For instance, reduction of  
189 aryl diazonium salts forms radical anions that covalently bind with the carbon surface<sup>33</sup>.

190 Barring some exceptions, bare gold is not a suitable electrode for PFE. However, gold electrodes have  
191 surface chemistry that can be controlled by forming self-assembled monolayers (SAMs) of thiol-  
192 derivatives, where the thiols form a stable gold-thiol bond<sup>34-37</sup>. This enables careful optimisation of  
193 the electrode surface chemistry by forming reproducible hydrophilic/hydrophobic surfaces with  
194 negative and/or positive groups. Gold electrodes can be crystalline, ultrasmooth, rough or prepared  
195 from nanoparticles. The exact geometry of the gold electrode affects the structure of the SAM<sup>34</sup>, which  
196 affects the protein film formation and PFE results. PFE is typically performed with freshly prepared  
197 SAMs. A drawback of using modified gold electrodes is that SAMs are typically formed over many  
198 hours, limiting the number of experiments that can be performed in a day.

199 ITO electrodes are increasingly being used. They are optically transparent, enabling simultaneous  
200 absorbance spectroscopy or photobioelectrochemistry. To increase the electrode area and roughness,  
201 ITO nanoparticles can be used to create mesoporous surfaces with greater opportunity for protein  
202 adsorption<sup>38-40</sup>. Preparation methods include using polystyrene beads as a template, around which the  
203 ITO nanoparticles are deposited. This results in more highly ordered<sup>38,41</sup>, honeycomb-like electrode  
204 materials than direct electrophoretic deposition<sup>40</sup>.

### 205 ***Film preparation***

206 The protein film is typically prepared by briefly incubating the freshly polished or prepared WE surface  
207 in a small volume of protein solution, just enough to wet the surface, typically  $\mu\text{M}$  concentration.  
208 Longer incubation times may be used with more dilute protein solutions. Loosely bound material may  
209 be removed from the WE surface by rinsing with an appropriate pH buffered-electrolyte solution  
210 before the electrode is introduced to the electrochemical cell. It is advised that the film forming  
211 solution not be allowed to dry on the WE. If the solution does dry on the WE, it can result in behaviour  
212 that is difficult to reconcile with established biochemical assays, presumably due to partial or complete  
213 loss of protein structure on adsorption.

### 214 ***Anaerobicity and temperature***

215 For experiments with applied WE potentials of approximately  $-0.1\text{ V}$  vs SHE and lower, oxygen needs  
216 to be removed from the electrolyte, unless the aim is to measure oxygen interaction with the protein  
217 film. For stationary electrodes, purging the electrolyte with nitrogen or argon gas is typically sufficient.  
218 For lengthy experiments ( $>$  hours), gas that has been humidified by bubbling through water can be

219 used to reduce solution evaporation, which would change the ionic strength or pH of the electrolyte.  
220 When using a RDE, anaerobicity can be achieved with closed electrochemical cells, as the rotating  
221 electrode stirs the electrolyte, rapidly drawing in air or gas. Closed RDE systems can be challenging to  
222 design. Open systems may be preferred and are most readily used within a glove box — a N<sub>2</sub>-filled  
223 chamber — to ensure anaerobic conditions.

224 Temperature is an important parameter because it is a primary determinant of reaction rate.  
225 Temperature is most conveniently controlled by placing the electrochemical cell in a temperature-  
226 controlled solution. Commercial or tailor-made electrochemical cells can be designed with an external  
227 water jacket, where the temperature is set with a circulating water bath. However, the potential of  
228 the RE is temperature dependent. For accurate control of the applied potential, the RE can be placed  
229 in a side-arm of the cell with its own temperature-controlled water jacket, **FIG. 2B,C**.

### 230 **Software**

231 All commercial potentiostats come with software to control the hardware. This software is often able  
232 to perform a basic analysis of voltammograms and amperograms, but capabilities are very limited.  
233 A versatile, freely available software is QSoas<sup>42-44</sup>. QSoas enables basic data analysis, such as  
234 smoothing and baseline subtraction capabilities to remove non-Faradaic currents. QSoas also allows  
235 non-linear curve fitting, creating a flexible fitting platform to analyse catalytic waves with complex  
236 kinetic models. QSoas is still being expanded, with recent additions including calculation of redox  
237 peaks at increasing scan rate.

238 Electronic noise can often be eliminated by careful design and maintenance of the electrochemical  
239 equipment and its location<sup>18</sup>. If noise persists, its contribution to the measured data can be lowered  
240 in several ways<sup>18</sup>. Random noise can be removed by signal averaging applied to consecutive steady-  
241 state measurements. Regular, periodic noise can be removed by fast Fourier transform techniques,  
242 which are included in the controlling software or QSoas. If such methods are used, it is important to  
243 inspect the data carefully to ensure that key information hasn't been distorted.

### 244 **Further considerations**

245 The experimental and equipment requirements outlined above are for basic PFE experiments.  
246 However, there are many insightful and exciting examples where PFE is expanded beyond the basic  
247 setup. These may require adjustments to the electrochemical cell and electrodes or additional  
248 equipment. Examples include the use of microelectrodes<sup>45,46</sup>, combining PFE with spectroscopy<sup>27,47-52</sup>,  
249 using high or low (< 0 °C) temperatures<sup>53</sup> or specialised gas mixtures. A full discussion is beyond the  
250 scope of this Primer, but three options could be considered when purchasing a potentiostat. All  
251 potentiostats perform basic CV and CA, but more advanced methods, such as electrochemical  
252 impedance spectroscopy, are not standard. Impedance spectroscopy can be useful when studying  
253 SAM formation on gold WEs. When studying catalysis, a RRDE can be useful<sup>54</sup>, but requires a  
254 potentiostat with the ability to measure two or double WEs. Finally, when using microelectrodes, the  
255 ability to accurately measure pA and sometimes fA currents is necessary.

256

## 257 **RESULTS**

258 A few scenarios can provide the basis to describe many redox-active proteins.. This section details the  
259 corresponding Faradaic currents and the information that can be extracted. Because the  
260 experimentally measured currents include both Faradaic and non-Faradaic contributions, it is  
261 important to reiterate that the latter must be subtracted from the measured currents prior to analysis,

262 **FIG. 3A,B.** This subtraction may make use of baseline currents measured in an identical experiment  
 263 without adsorbed protein<sup>55</sup>. Alternatively, the non-Faradaic currents may be modelled using QSoas<sup>42-</sup>  
 264 <sup>44</sup>. Good practice is to always measure the baseline response. This measurement enables informed  
 265 modelling of the charging currents and minimises the likelihood that Faradaic currents from  
 266 contaminants or additives reacting directly at the electrode will be mistaken as from the protein of  
 267 interest<sup>8,55-57</sup>.

### 268 **Mapping out half-reactions**

269 Reversible oxidation and reduction of an adsorbed protein by varying the WE potential can be  
 270 described by a half-reaction:  $Ox + ne^- \rightarrow Red$ . When this process is uncomplicated by slow interfacial  
 271 electron transfer kinetics or coupling with a chemical reaction, cyclic voltammetry reveals peaks that  
 272 are superposed on the non-Faradaic baseline response. These peaks are mirror images along the  
 273 potential axis, **FIG. 3A,B**. Peaks detected when sweeping to increasingly positive WE potentials  
 274 correspond to protein oxidation and have positive currents. Peaks with negative currents that are  
 275 measured by sweeping to increasingly negative WE potentials describe cofactor reduction. Such peaks  
 276 are sometimes termed non-catalytic because they do not arise from redox catalysis. When  
 277 interpreting each non-catalytic peak, the current magnitude,  $|i|$ , can be described by<sup>15,58</sup>:

278 Equation (1)

$$279 \quad |i| = \frac{\exp\left(\frac{nF}{RT}(E - E^0)\right)}{\left(1 + \exp\left(\frac{nF}{RT}(E - E^0)\right)\right)^2} \cdot \frac{n^2 F^2 v A \Gamma}{RT}$$

280 where  $E$  is the WE potential,  $E^0$  the reduction potential and  $n$  the number of electrons transferred in  
 281 the corresponding half-reaction,  $F$  = Faraday's constant,  $R$  = gas constant,  $T$  = absolute temperature,  
 282  $v$  = voltametric scan rate (V/s),  $A$  = WE surface area (cm<sup>2</sup>), and  $\Gamma$  = electroactive redox protein  
 283 coverage (moles/cm<sup>2</sup>). The peak currents ( $i_p^{ox}$  and  $i_p^{red}$ , **FIG. 3A**) have equal magnitude. The  
 284 potentials of maximum current ( $E_p^{ox}$  and  $E_p^{red}$ ) are those of  $E^0$ . The stoichiometry of electrons  
 285 transferred in the half-reaction is defined by the half-height peak width ( $W_{1/2}$ ) using Equation (2).

286 Equation (2)

$$287 \quad W_{1/2} = \frac{2RT}{nF} \ln(3 + 2\sqrt{2})$$

288 At 25°C,  $W_{1/2} = 90$  mV for  $n = 1$ , **FIG. 3C** green, and  $W_{1/2} = 45$  mV for  $n = 2$ , **FIG. 3C** orange. However,  
 289 pure  $n = 2$  reactions are rarely observed in proteins. More often cofactors — such as flavin,  
 290 molybdenum and tungsten — are described by two consecutive  $n = 1$  half-reactions that link the  
 291 oxidised, half-reduced and fully reduced levels. For this scenario, equations relating the peak shape  
 292 and  $W_{1/2}$  to the separation of reduction potentials have been presented<sup>59</sup>. **FIG. 3D** illustrates how the  
 293 form of the non-catalytic peaks is defined by the relative reduction potential values for the consecutive  
 294 half-reactions in REF<sup>59</sup> (page 147). In practice, small deviations from the ideal descriptions are often

295 seen. For example,  $E_p^{ox}$  and  $E_p^{red}$  may differ slightly such that  $E^\circ$  is reported as the average of the  
296 measured values.

297 Because the protein film is comprised of a finite number of molecules and cofactors, the Faradaic  
298 current drops to zero when a redox reaction is complete, **FIG. 3**. The peak area defines the moles of  
299 electroactive redox cofactor ( $A.\Gamma$ ) in the protein film through Equation (3)

300 Equation (3)

$$301 \quad A.\Gamma = \frac{\Pi}{nFv}$$

302 where  $\Pi$ , the voltammetric peak area, has units of Amps.Volts (= Coulombs.Volts/sec). The areas of  
303 the oxidation and reduction peaks will be equal for a fully reversible redox process.

304 For proteins with more than one half-reaction, each reaction contributes Faradaic currents and the  
305 responses are additive<sup>12,48,60-64</sup>. For the example presented in **FIG. 3B**<sup>12</sup>, the widely spaced peaks  
306 immediately reveal three half-reactions. A cooperative  $n = 2$  process appears as a prominent and  
307 narrow pair of peaks at more negative WE potentials, compared to an equivalent number of  $n = 1$   
308 centres at more positive WE potentials. This distinction arises because the current magnitude varies  
309 as  $n^2$  (Equation 1);  $W_{1/2}$  varies as  $90/n$  (Equation 2); and the peak area as  $\Pi$  (Equation 3). Multiple half-  
310 reactions are readily detected when  $E^\circ$  values are separated by  $> 0.1$  V, **FIG. 3C** (dark green). When  $E^\circ$   
311 values are more similar, the voltammogram may suggest a single redox centre, for example a single  
312 peak with  $W_{1/2} = 90$  mV for two  $n = 1$  centres with identical  $E^\circ$ , **FIG. 3C** (purple). In such situations fine  
313 structure within non-catalytic peaks may be indicative of multiple overlapping contributions. The  
314 ability of multiple half-reactions to describe non-catalytic peaks can be readily assessed by modelling  
315 the Faradaic currents using the equations presented above with  $E^\circ$  and  $n$  as variables. Such modelling  
316 can be performed in a spreadsheet programme or with iterative fitting using QSoas<sup>42-44</sup>. In parallel to  
317 such analysis, CV can be performed at a different pH values.  $E^\circ$  of one half-reaction may respond  
318 differently to pH, causing multiple, distinct non-catalytic peaks to be resolved for both oxidation and  
319 reduction.

320 The shape of non-catalytic peaks depends on the scan rate, **FIG. 4A**. For half-reactions with the form  
321  $Ox + ne^- \rightarrow Red$ , the descriptions above are relevant at low scan rates, typically  $< 30$  mV s<sup>-1</sup>. At higher  
322 scan rates, the oxidation and reduction peaks become smeared across the potential axis and peak  
323 currents are smaller than predicted by extrapolating values measured at low scan rates, **FIG. 4A**. As  
324 the scan rate increases, the peak currents remain approximately equal ( $i_p^{ox} \approx |i_p^{red}|$ ),  $E_p^{ox}$  becomes  
325 increasingly positive and  $E_p^{red}$  increasingly negative. This is because interfacial electron transfer  
326 between the protein and WE becomes -slow on voltammetric timescale. The interfacial electron  
327 transfer rate constant ( $k_{het}^o$ ) can be extracted from plots of  $E_p^{ox}$  and  $E_p^{red}$  versus  $\log(\text{scan rate})$  using  
328 procedures<sup>4,58,65</sup> based on an exponential increase of rate with overpotential, Butler-Volmer  
329 equation<sup>15</sup>, or Marcus theory, which is more appropriate for protein cofactors with low reorganisation  
330 energy<sup>20</sup>. Such plots, **FIG. 4B**, are referred to as Trumpet Plots because the deviation of  $E_p^{ox}$  and  $E_p^{red}$   
331 from  $E^\circ$  has approximately equal magnitude but opposite sign<sup>66</sup>. More complex behaviour<sup>67</sup> is  
332 observed for centres, such as flavins, where consecutive  $n = 1$  reactions occur, sometimes separated  
333 by a protonation event.



### 334 **Redox-driven ligand binding and unbinding**

335 CV provides several ways to identify and characterise redox-driven chemistry, such as ligand binding  
336 and unbinding. One approach is to study the scan rate dependence of the non-catalytic peaks and look  
337 for change in the relative magnitudes of  $i_p^{ox}$  and  $i_p^{red}$ , **FIG. 4C**<sup>68</sup>. For this example,  $i_p^{ox}$  decreases  
338 relative to  $|i_p^{red}|$  at higher scan rates. The reduction peak remains well-defined. By contrast, the  
339 oxidation peak is increasingly smeared towards more positive potentials. The corresponding plot of  
340  $E_p^{ox}$  and  $E_p^{red}$  versus log (scan rate) no longer resembles a trumpet, **FIG. 4D**. CV at the higher scan  
341 rates reveals that reduction is fast, but re-oxidation is slower. Such behaviour is indicative of a  
342 chemical change in the reduced state, which is slow to reverse, limiting the rate of re-oxidation. Using  
343 the corresponding reaction scheme ( $Ox + ne^- \leftrightarrow Red \leftrightarrow Red^*$ ), rate constants can be quantified by  
344 modelling the scan rate dependence of the non-catalytic peaks<sup>20,22,68-71</sup>.

345 A second way to identify ligand binding and unbinding is to study the non-catalytic peaks at low scan  
346 rates in solutions of different ligand concentration (for proton binding this is different pH), **FIG. 4E**. For  
347 conditions where  $i_p^{ox} \approx |i_p^{red}|$  and  $E_p^{ox} \approx E_p^{red}$  the observed reduction potential  $E^{obs} = (E_p^{ox} + E_p^{red})/2$   
348 is dependent on ligand concentration, **FIG. 4F**. To define the thermodynamic parameters describing  
349 ligand binding, the data is fitted to a relevant equation<sup>9,68,69,72</sup>. For example, Equation (4) describes the  
350 behaviour for ligand binding to an  $n = 1$  redox site:

351 Equation (4)

$$352 \quad E^{obs} = E^o + \frac{RT}{F} \ln \left( \frac{1 + \frac{[L]}{K_d^{Red}}}{1 + \frac{[L]}{K_d^{Ox}}} \right)$$

353 where  $E^o$  is the reduction potential in the absence of a ligand,  $[L]$  is ligand concentration,  $K_d^{Ox}$  and  
354  $K_d^{Red}$  are dissociation constants for ligand binding to the oxidised and reduced states, respectively,  
355 **FIG. 4G**. In the limit that  $[L] \gg K_d^{Ox}$  and  $K_d^{Red}$ , the value of  $E^{obs}$  is equal to the reduction potential of  
356 the ligand bound redox cofactor,  $E^L$ , **FIG. 4G**.

357 Redox-coupled processes can occur on timescales much longer than a single cyclic voltammogram. In  
358 this situation, the chemistry and rates can be quantified by recording cyclic voltammetry continuously  
359 at a constant scan rate. The appearance of peaks due to the product and disappearance of peaks due  
360 to the reactant will be observed<sup>73,74</sup>.

### 361 **Redox catalysis**

362 During PFE in the presence of a catalytic substrate, the oxidation state of an adsorbed enzyme changes  
363 when the substrate is transformed to product. The WE acts as a redox partner to the enzyme, restoring  
364 the initial state of the enzyme, enabling further rounds of catalysis. Electrons are no longer confined  
365 to the protein film and a continuous flow of Faradaic current reports the rate of catalysis by the  
366 adsorbed film. This Faradaic current is referred to as the catalytic current.

367 When formation of an oxidised product is irreversible — unidirectional catalysis — and substrate  
 368 binding depends on prior oxidation of the active site, the fraction of molecules that are oxidised, able  
 369 to bind a substrate and complete the catalytic cycle is defined by the WE potential through the Nernst  
 370 equation<sup>75</sup>. The corresponding CV, **FIG. 5A**, reports a sigmoidal increase in positive catalytic current  
 371 when sweeping from more negative to more positive WE potentials. Similarly, CV of an adsorbed  
 372 enzyme performing unidirectional reductive catalysis reports a sigmoidal increase in negative catalytic  
 373 current on sweeping to more negative WE potentials, **FIG. 5B**. When the catalytic current-potential  
 374 profiles are independent of scan direction and scan rate (typically < 20 mV s<sup>-1</sup> in PFE) steady-state  
 375 catalysis is described through Equation (5)<sup>8,76</sup>:

Equation (5)

$$377 \quad |i_{cat}(E)| = \frac{i_{lim}}{1 + \exp\left(\pm \frac{n_{cat}F}{RT}(E_{hw} - E)\right)}$$

378 Here,  $i_{cat}(E)$  is the catalytic current for WE potential  $E$ ;  $i_{lim}$  is the maximum catalytic current  
 379 magnitude;  $i_{lim}^{ox}$  for oxidative catalysis and  $i_{lim}^{red}$  for reductive catalysis, **FIG. 5A,B**.  $E_{hw}$  is the half-wave  
 380 potential, the potential where the current is half of  $i_{lim}$ ;  $n_{cat}$  relates to the steepness of the catalytic  
 381 wave and the bracketed term is positive for oxidation and negative for reduction. The values of  $E_{hw}$   
 382 and  $n_{cat}$  reveal the subtleties of redox catalysis, for example, the consequences of redox equilibration  
 383 through a chain of electron transfer sites, as illustrated in **FIG. 1A**. The value of  $i_{lim}$  provides a direct  
 384 measure of the maximum rate of catalysis by the protein film through the relationship  $i_{lim}/F =$   
 385 (Coulombs/sec) ÷ (Coulombs/mole  $e^-$ ) = mole  $e^-$ /sec.

386 PFE of redox catalysis can provide insight into rate defining events intrinsic to the catalytic cycle of the  
 387 enzyme. These events may be redox transformation of substrate in the active site, substrate binding  
 388 to the enzyme, or product release from the enzyme. However, before PFE is interpreted in the context  
 389 of enzyme mechanism, it is important to understand that rate defining events in catalytic PFE may also  
 390 be defined by interfacial electron transfer, or delivery of substrate to the electrode via mass transport,  
 391 **FIG. 5C**. Limitations due to slow electron exchange between the WE and protein can be revealed<sup>77</sup> by  
 392 catalytic currents at high driving force, for instance at WE potentials significantly more negative or  
 393 positive than the reduction potential of the substrate-product couple. For these potentials, the  
 394 catalytic current magnitude has residual slope, **FIG. 5D**, instead of a plateau described by  $i_{lim}$ , **FIG.**  
 395 **5A,B**. The residual slope arises due to contributions from enzymes with low rates of interfacial electron  
 396 transfer compared to the enzyme turnover number,  $k_{cat}$ . As a result, the slope is greater when enzyme  
 397 activity is higher. Lowering the temperature, **FIG. 5D**, or substrate concentration can reduce the  
 398 limitations from slow interfacial electron transfer<sup>77</sup>.

399 Limitations to the catalytic rate from relatively slow substrate delivery to the adsorbed enzyme are  
 400 readily detected and sometimes overcome with a RDE. The RDE alleviates mass transport limitations  
 401 by forced convection<sup>15</sup>. Catalytic currents that are free from mass transport limitations will be  
 402 independent of the electrode rotation rate. When this cannot be achieved experimentally, catalytic  
 403 currents measured at different rotation rates may be extrapolated to the catalytic current observed  
 404 at infinitely high electrode rotation rate. This is typically done through a Koutecky-Levich plot with  
 405 inverse catalytic current versus inverse square root of the rotation rate, presented as angular velocity,  
 406 **FIG. 5E**<sup>78,79</sup>. Another approach for alleviating diffusion related limitations is to reduce enzyme loading  
 407 ( $\Gamma$ ) on the electrode surface<sup>80</sup>. This increases the diffusion layer for substrate molecules that reach the

408 enzyme, by allowing hemispherical rather than planar diffusion<sup>81</sup>. Using an ultramicroelectrode as the  
409 WE can achieve the same outcome<sup>82,83</sup>.

410 When  $i_{lim}$  is defined by the intrinsic properties of the enzyme it can be related to the substrate  
411 concentration, [S], through Equation (6), the electrochemical form<sup>8,9,84</sup> of the Michaelis-Menten  
412 expression<sup>17</sup> :

413 Equation (6)

$$414 \quad i_{lim} = \frac{nFA\Gamma k_{cat}[S]}{K_M + [S]}$$

415 where  $n$  is the number of electrons needed to convert the substrate to product;  $K_M$  is the Michaelis  
416 constant; and  $k_{cat}$  is the turnover number of the enzyme. Often, the amount of electroactive enzyme,  
417  $\Gamma$ , is unknown since non-catalytic peaks cannot be discerned. However, the variation of  $i_{lim}$  with [S]  
418 enables quantification of  $K_M$ . This is straightforward when there is very little change of  $\Gamma$  during an  
419 experiment. To check changes in  $\Gamma$ , the enzyme coated electrode should be returned to standard  
420 conditions and  $i_{lim}$  remeasured at different time points in the experiment. When a time-dependent  
421 decay can be quantified, it is often first order<sup>79,85,86</sup>.  $i_{lim}$  can be converted to values at time zero using  
422 the first order decay rate and the known time  $i_{lim}$  was measured. The time zero currents can be  
423 included in Equation (6) to quantify  $K_M$ . Such approaches are readily extended to assess changes in  
424 redox catalysis due to variations in pH and inhibitor concentration. Characteristic changes in  $K_M$  and  
425  $i_{max}$  ( $\propto k_{cat}$  for conditions where [S]  $\gg K_M$ ) are then interpreted through standard descriptions<sup>17</sup> of  
426 enzyme catalysis.

427 CA provides a powerful complement to CV when studying redox catalysis. Variations in  $i_{lim}$  with  
428 substrate or inhibitor concentration can be defined by holding the WE at an appropriate potential and  
429 performing sequential additions of the reagent to the electrochemical cell, **FIG. 5F**. During steady-  
430 state catalysis, the catalytic current will be constant and independent of time following each addition.  
431 When inhibitor addition leads to time-dependent changes, it suggests relatively slow inhibitor binding  
432 and unbinding<sup>87-90</sup>.

433 CV can report catalytic currents for both oxidation and reduction. If the adsorbed enzyme catalyses a  
434 reaction in both directions — bidirectional catalysis<sup>91,92</sup> — the potential of zero current directly relates  
435 to the reduction potential ( $E^0$ ) of the substrate-product couple through the Nernst equation<sup>92-94</sup>.  
436 Steady-state catalytic current profiles sometimes have additional contributions that describe a boost,  
437 or attenuation, of catalysis with increasing driving force. Different explanations have been offered for  
438 this behaviour<sup>8</sup>.

439

## 440 APPLICATIONS

441 Building on the key concepts to interpret PFE and characterise protein redox chemistry, this section  
442 provides selected examples that explore these ideas in greater detail. Case studies illustrate how to  
443 tailor the WE for direct electron exchange with proteins, the utility of RRDEs, and the benefits of multi-  
444 disciplinary studies when interpreting complex non-typical measurements. Examples are presented  
445 within a wider discussion of three research areas where PFE is making leading contributions.

### 446 Biosensing

447 In PFE, the catalytic current for an enzyme-catalysed reaction depends on the substrate concentration,  
448 Equation (6). Consequently, PFE can quantify substrate concentration, which underpins the operation  
449 of electrochemical biosensors<sup>95-99</sup>. Biosensors operating in this way are sometimes called third  
450 generation biosensors. Earlier generations used redox mediators or co-substrates to shuttle electrons  
451 between the WE and enzyme. However, small-molecule mediators can diffuse away from the WE  
452 during measurements. As a result, electron exchange with the enzyme is compromised and catalytic  
453 currents no longer have a simple dependence on the substrate concentration. Biosensors based on  
454 direct electron transfer benefit from not requiring redox mediators or co-substrates<sup>96</sup>. The challenge  
455 of third generation biosensors is to establish stable electro-active enzyme populations that undergo  
456 facile electron transfer with the WE. To address this challenge, different electrode materials and  
457 surface functionalization have been explored and a variety of enzymes have been tested for their  
458 ability to directly exchange electrons with these electrodes<sup>100-102</sup>.

### 459 **Case Study 1**

460 Cellobiose dehydrogenase (CDH) is an enzyme that oxidises lactose, providing a basis for  
461 electrochemical biosensing of a disaccharide that is prevalent in dairy products and causes symptoms  
462 of lactose intolerant. CDH<sup>103</sup> is a monomeric enzyme, **FIG. 6A**, consisting of a catalytic dehydrogenase  
463 domain (DH) with strongly a bound flavin adenine dinucleotide in the active site, and a cytochrome  
464 domain (CYT) that carries a *b*-type heme. A flexible linker region connects the DH and CYT domains.  
465 When CDH is adsorbed on unmodified, solid gold WEs, electrons generated by lactose oxidation in the  
466 DH domain are shuttled via CYT to the WE. To improve the long-term stability and catalytic current  
467 density of the biosensor, positively charged polyethyleneimine-coated gold nanoparticles (PEI-AuNPs)  
468 can be deposited on the WE prior to CDH adsorption<sup>104</sup>, **FIG. 6A**. The nanostructured material  
469 increases the WE surface area available for enzyme adsorption. In addition, the positively charged PEI  
470 binds and orientates the negatively charged CYT domain to favour direct electron exchange with the  
471 WE. CV of CDH adsorbed on PEI-AuNPs, **FIG. 6B**, reports well-defined, reversible peaks due to redox  
472 cycling of the *b*-heme in the CYT domain. Variation of the peak potentials with scan rate gives a typical  
473 trumpet plot. From this, the rate constant ( $k_{het}^o$ ) for electron transfer between CYT and PEI-AuNPs can  
474 be calculated as 40 s<sup>-1</sup>. The rate is higher than electron transfer between DH and CYT domains (30 s<sup>-1</sup>),  
475 meaning the catalytic oxidation currents measured in the presence of lactose, **FIG. 6C**, are fully  
476 determined by the intrinsic properties of the enzyme. Catalytic currents vary linearly with lactose  
477 concentrations 1–100 μM, **FIG. 6D**. Fitting to Equation (6) gives a  $K_M$  of 0.2 mM lactose. The limit of  
478 detection is 0.33 μM lactose. CA establishes that the catalytic currents decrease by only 5.3% during  
479 ~300 continuous injections of lactose over 24 hours, indicating excellent long-term stability.

### 480 **Energy conversion**

481 Many redox enzymes evolved to harness energy from the environment, either from sunlight during  
482 photosynthesis or chemicals during respiration. PFE replaces an enzyme's natural redox partner with  
483 a WE, creating opportunities for sustainable energy conversion. Examples include transfer of chemical  
484 to electrical energy in biofuel cells<sup>105,106</sup> and the conversion of light to electricity in biophotovoltaic  
485 devices<sup>39,41,52,107</sup>. For converting light to electricity, Photosystem II (PSII) attracts much interest. PSII is  
486 a membrane spanning protein complex that produces electrons, oxygen and protons simultaneously  
487 via a water-splitting photoreaction<sup>25,108</sup>. PFE readily measures the light-triggered photocurrents  
488 through CA by holding the biophotoelectrode at a desired potential and exposing it to alternating  
489 light/dark regimes. Results<sup>109</sup> comparing the WE behaviour with and without immobilized PSII are  
490 illustrated in **FIG. 7A**, where PSII was linked to a SAM coated gold WE. The SAM was terminated by  
491 nickel-nitrilotriacetic acid functionalities, enabling a direct link to PSII through a polyhistidine-tag.  
492 Another approach<sup>110</sup> to immobilize PSII uses electrostatic interactions at ITO WEs, **FIG. 7B**. PSII carries

493 a permanent dipole moment, bringing a positive charge to the region of the protein where electron  
494 exchange with the WE occurs. Consequently, ITO WEs coated with a carboxylate (negatively)  
495 terminated SAM produces higher photocurrents than equivalent WEs with no SAM or an amine  
496 (positively) terminated SAM. Photocurrents can be further enhanced and show greater stability when  
497 the carboxylate terminated SAMs incubated with PSII are exposed to covalent coupling molecules,  
498 such as carbodiimide and N-hydroxy succinimide.

499

## 500 **Case Study 2**

501 Mechanistic insights into the photoreactivity of PSII by PFE can be achieved using a RRDE<sup>54</sup> and  
502 potentiostat to independently control the potential applied at the disk and ring WEs. To study water  
503 oxidation, PSII was adsorbed on a glassy carbon disk electrode, **FIG. 7C** (centre) and held at 0.5 V vs  
504 SHE in a nitrogen-purged electrolyte solution. Positive photocurrents report light-driven oxidation by  
505 PSII, **FIG. 7C** (left red). A platinum ring electrode, held at -0.5 V versus SHE, provides direct  
506 quantification of oxygen liberated by PSII as a reductive current, **FIG. 7C** (left blue). Quantifying the  
507 photocurrent ratios reveals that the majority (>94%) of electrons delivered to the electrode are used  
508 for water oxidation by PSII. A separate experiment performed in the presence of oxygen detected  
509 light-driven reduction currents from the PSII coated disk electrode, accompanied by oxidative  
510 photocurrents at the ring electrode held at 0.9 V vs SHE **FIG. 7C** (right). Further experiments<sup>54</sup>  
511 established two pathways for oxygen reduction to H<sub>2</sub>O<sub>2</sub> via a PSII generated superoxide (O<sub>2</sub><sup>•-</sup>).

## 512 **Elucidating mechanisms of redox catalysis**

513 Michaelis-Menten descriptors of steady-state redox enzyme catalysis are readily defined by PFE. PFE  
514 also provides a powerful route to resolve catalytic mechanisms and properties of catalytic  
515 intermediates. For example, CV with substrate concentrations in large excess of  $K_M$  enables  
516 examination of electron transfer within the enzyme-substrate complex when scan rates are  
517 sufficiently fast to outrun the catalytic cycle<sup>111</sup>. For studies of electron transfer within covalent enzyme  
518 adducts, the presence of the covalent adduct can be confirmed by mass spectrometry immediately  
519 before adsorption on the electrode and on recovery of the sample from the electrode after CV<sup>60</sup>.

520 Arguably, the most significant contributions of PFE to understanding enzyme mechanisms are in  
521 dissecting the redox driven activation and deactivation of active centres, and elucidating molecular  
522 determinants of substrate access to deeply buried active centres. Such studies highlight how complex  
523 behaviours observed by CV as hysteretic catalytic current-potential profiles can be resolved through  
524 CA<sup>87,88,112,113</sup>. An illustrative example is the behaviour of *Aquifex aeolicus* NiFe hydrogenase, which  
525 catalyses H<sub>2</sub> oxidation<sup>88</sup>. The CV, **FIG. 8A**, shows a peak of positive catalytic current corresponding to  
526 a maximum H<sub>2</sub> oxidation rate. Sweeping to more positive WE potentials increases the rate of H<sub>2</sub>  
527 oxidation from the active enzyme and simultaneously drives the oxidative formation of inactive  
528 enzyme. The activity of the enzyme is recovered by sweeping to more negative potentials, **Fig. 8A**,  
529 meaning oxidative inactivation reverses on enzyme reduction. Activation and inactivation are slow on  
530 the voltammetric timescale — an experiment at 0.3 mV/s takes about an hour — because the catalytic  
531 currents are smaller when sweeping to more negative potentials than when sweeping to more positive  
532 potentials. CA exposed the hydrogenase to potentials that inactivated (+65 mV) and then re-activated  
533 (-60 mV) the hydrogenase such that the catalytic current decreased and then increased, **FIG. 8B**.  
534 Variations in the catalytic current magnitude are directly proportional to the fraction of active enzyme.  
535 Rates of activation and deactivation can be quantified by fitting to a scheme that describes the  
536 reversible interconversion of active and inactive forms<sup>88</sup>.

### 537 **Case Study 3**

538 PFE has contributed to multi-disciplinary studies<sup>89,90,114,115</sup> of CO binding to and inhibition of  
539 *Desulfovibrio fructosovorans* NiFe hydrogenase. The crystal structure of this enzyme has a  
540 hydrophobic channel that allows H<sub>2</sub> from the surrounding solution to diffuse to the NiFe-cofactor  
541 containing active site, **FIG. 8C**. The same channel allows CO to reach the active site and act as a  
542 competitive inhibitor of H<sub>2</sub> oxidation. Insights into how the channel affects CO diffusion rates in the  
543 protein were provided by CA of NiFe hydrogenase adsorbed on a rapidly rotating electrode in an  
544 electrochemical cell continuously bubbled with H<sub>2</sub> gas<sup>90</sup>. Introducing an aliquot of CO to the enzyme  
545 produced immediate inhibition, followed by a slow recovery of activity as CO was flushed out of the  
546 electrochemical cell, **FIG. 8D** (left). Gas binding and release rates were calculated from the  
547 corresponding amperograms.

548 Changing residues Valine74 and Leucine122 in the gas channel to Isoleucine and Phenylalanine  
549 respectively, **FIG. 8C**, reduced the CO diffusion rate within the gas channel more than 10-fold<sup>90</sup>, **FIG.**  
550 **8D** (right). The same mutations had minimal impact on the catalytic rate of H<sub>2</sub> oxidation,  
551 demonstrating that the enzyme may be engineered to resist gaseous inhibition and could be applied  
552 as an alternative to platinum catalysts in H<sub>2</sub> conversion technology. Furthermore, gas diffusion rates  
553 are not simply correlated with the main gas channel width defined by X-ray crystallography, **FIG. 8C**.  
554 Molecular dynamics calculations point towards CO diffusion rates being controlled at multiple  
555 locations within the gas channel<sup>115</sup>.

556

### 557 **REPRODUCIBILITY AND DATA DEPOSITION**

558 For a given protein, reproducibility in PFE relates to the data collected with a single film and from  
559 different films. Use of data repositories has not been adopted, but published results are typically  
560 available in accord with open access agreements.

561 Repeatability is related to several factors. PFE for a given protein is critically dependent on instrument  
562 parameters, for example, scan rate and vertex potentials for CV, and poisoning potential and time for  
563 CA. The WE rotation rate and temperature may also be defining parameters when studying redox  
564 catalysis. If the protein film is prepared on a cold WE, care should be taken to ensure equilibrium  
565 occurs at the desired measurement temperature before data collection. Non-reproducible values of  
566  $E_p$  and  $E_{hw}$  can arise from poorly maintained Res or gas bubbles in the electrochemical cell.

567 Unwanted and irreproducible contributions can arise from trace amounts of redox active impurities.  
568 The method is sensitive, with redox signals visible for quantities < pmol/cm<sup>2</sup>. All solutions should be  
569 carefully defined using water and reagents of the highest possible purity. Careful cleaning of glassware  
570 with, for instance, nitric acid, aqua regia, or fuming sulfuric acid is sometimes required to prevent  
571 unwanted signals. Protein adsorption may be influenced by co-adsorbing impurities regardless of their  
572 redox activity.

573 For a given sample and measurement condition, variations between separately prepared films include  
574 differences in charging current, electroactive coverage and desorption rates. Such discrepancies can  
575 be pronounced for different WE treatments. For example, extended application of a certain potential  
576 to the electrode can change the electrode surface and protein behaviour. Prolonged poisoning of the WE  
577 after the protein film has formed can also alter the response by changing the state of an enzyme or  
578 interface. However, PFE should report the same behaviour when freshly prepared films are subject to  
579 an equivalent series of chemical and measurement conditions. For example, values for  $E_p$ ,  $W_{1/2}$  and the

580 ratio  $i_p^{ox}/i_p^{red}$  should be consistent for CV that defines redox couples and ligand binding events. During  
581 redox catalysis, critical features of the current-potential profile, such as  $E_{hw}$  and  $n_{cat}$ , should be  
582 consistent. These parameters can be hard to accurately define when the population of electroactive  
583 protein is low, making accurate subtraction of the charging current from the measured current  
584 challenging. This challenge is amplified when the baseline deviates significantly from the theoretical  
585 behaviour<sup>15</sup> of a plate capacitor. For example, broad peaks due to oxidation or reduction of surface  
586 groups are a known complication of working with graphite electrodes. The most appropriate approach  
587 to baseline subtraction is still a topic of debate.

588 PFE will ideally provide the same description of redox chemistry for two or more independently  
589 purified samples of a given protein. Unintended and non-reproducible signals can arise from cofactors  
590 released from adsorbed or denatured proteins. This is a frequent complication in studies of  
591 flavoproteins using graphite electrodes<sup>116</sup>. The extent of adsorption may depend on the presence or  
592 identity of an affinity tag introduced to facilitate protein purification<sup>117</sup>.

593

## 594 LIMITATIONS AND OPTIMISATIONS

595 Not all redox proteins can be studied by PFE. It is essential that the protein has at least one surface  
596 exposed redox centre that can act as a point of connection between the electrode and any additional  
597 redox centres in the protein, **FIG. 1A**. Establishing conditions to detect and optimise PFE is like finding  
598 the conditions for highly ordered protein crystallization ahead of structure resolution by X-ray  
599 diffraction. The chances of success are greater with small, soluble proteins due the high percentage  
600 of surface exposed redox cofactors compared to larger proteins.

601 Most electrode-protein interactions have a contribution from electrostatic interactions. The extent  
602 and orientation of protein adsorption can be modulated through changes in the pH and ionic strength  
603 of the protein-containing solution, the presence of a co-adsorbate, the choice of WE, and the  
604 functional groups in the SAM<sup>118</sup>. If initial experiments have no, or small, Faradaic signals then it is  
605 worth exploring different conditions to increase the electroactive population. For studies of redox  
606 enzymes, the catalytic currents are proportional to the product of enzyme concentration and turnover  
607 number (Equation 6). The chances of success are also increased for highly active enzymes. Because  
608 catalytic currents are larger than the corresponding non-catalytic peaks, sometimes by several orders  
609 of magnitude, it is always worth adding a substrate to experiments with redox enzymes to look for a  
610 catalytic response. Studies of redox catalysis are informative even when there are no detectable non-  
611 catalytic peaks.

612 The WE and composition of the pH buffered electrolyte solution places constraints on the explorable  
613 electrochemical potential window. As the majority of PFE is performed in aqueous solution, direct  
614 reduction of protons, leading to H<sub>2</sub> evolution at the WE, can result in large negative currents that mask  
615 currents from the protein of interest. Fortunately, proton reduction is slow at most WE materials  
616 specifically mentioned in this account, including gold electrodes with a well-formed SAM.  
617 Consequently, the currents appear only at large overpotentials with respect to the H<sup>+</sup>/H<sub>2</sub> couple. These  
618 currents tend to be smaller and appear at more negative potentials for measurements performed at  
619 more alkaline pH and faster scan rates. The limiting value of positive potential is typically defined by  
620 currents due to oxidation of anions from the electrolyte. It can be altered by changing the  
621 concentration or identity of the ions, for instance chloride versus sulphate or chlorate. When using a  
622 SAM-coated gold WE, the accessible potential window depends on the identity of the thiol and pH but

623 is typically -0.6 to +1.0 V vs SHE<sup>119,120</sup>. Reductive desorption of the SAM is minimised by using scan  
624 rates > 0.1 V/s.

625 Most PFE experiments aim to uncover the intrinsic properties of proteins relevant to biochemistry. To  
626 ensure that the PFE does not arise from a denatured protein or dissociated cofactor, behaviour  
627 reported by PFE should correlate with properties observed in complementary measurements<sup>121</sup>. For  
628 redox enzymes,  $K_M$  values are readily compared to those from the classical biochemical assays.  
629 Reduction potentials are typically compared to those defined by potentiometric titration of the  
630 protein in solution, although small differences (< 25 mV) can be observed as the environment of an  
631 adsorbed protein is not identical to that in solution. The currents measured in PFE report redox activity  
632 but do not define the chemical basis of those redox events. To confidently assign a reduction potential  
633 to a specific cofactor, and catalytic current to formation of a specific product, information from  
634 complementary methods is needed.

635

## 636 **OUTLOOK**

637 PFE has seen continuous developments, with advances in electrode materials, theory, methodology  
638 and in situ combination of PFE with spectroscopy and microscopy. Further improvements in these  
639 areas will continue to expand the applications of PFE.

640 For some applications, PFE is limited by low electroactive coverage due to non-optimal protein  
641 orientation, poor protein adsorption or because surface exposed redox co-factors are inaccessible for  
642 electron exchange with planar macroscopic WEs. These challenges are sometimes overcome by  
643 including conducting nanoparticles, for example carbon nanotubes, graphene oxide flakes, and gold  
644 and ITO nanoparticles. Nanoparticles have two important benefits. First, they increase the surface  
645 area of the WE, providing more sites for attachment and increasing protein coverage. A second benefit  
646 is that nanoparticles enable more interactions with the topologically rich surface of a redox protein.  
647 These versatile interactions mean nanoparticles can approach redox centres more closely than planar,  
648 macroscopic electrodes.

649 As shown in Case Study 1<sup>104</sup>, **FIG. 6A**, electrodes modified with nanoparticles before protein  
650 application can strongly enhance the electroactive coverage. In an alternative approach, protein  
651 samples can be mixed with nanoparticles and suspensions applied to the electrode. In the most  
652 extreme cases, the protein-nanoparticle composite material can be considered to have become the  
653 WE, with the underlying conducting material only used as a connector to the composite material. The  
654 resulting higher electroactive coverage has enabled in situ spectroscopy. Examples are hydrogenase  
655 studied under turn-over conditions using Fourier transform infrared spectroscopy<sup>122</sup> and redox co-  
656 factors characterised at various oxidation states with electron paramagnetic resonance  
657 spectroscopy<sup>123</sup> or electronic absorption spectroscopy<sup>48</sup>. Extending the use of spectroscopy in the  
658 future will greatly improve the understanding of PFE and expand its applications.

659 A drawback of using nanoparticle modified WEs when studying redox catalysis — particularly if thick  
660 ( $\mu\text{m}$ ) layers are used with proteins embedded in the nanoparticle layer — is that diffusion of substrates  
661 and products through nanoparticle films can be limited. Detailed descriptions of diffusion in such  
662 electrodes have yet to be established. However, experimental approaches that facilitate diffusion  
663 through nanoparticle layers are being developed. One example is hierarchically structured surfaces  
664 with micrometre-sized pores, engineered by templating or printing techniques<sup>38,124</sup>. Further  
665 developments to electrode materials will improve adsorption of electroactive protein and access to  
666 substrates. Electrocatalytic currents of > 1 mA/cm<sup>2</sup> have already been obtained<sup>125,126</sup>. Current densities



667 >> 10 mA/cm<sup>2</sup> could make PFE commercially relevant for biosynthesis of fuels and chemicals, but this  
668 would require improvements in the stability of the protein films, for example by grafting<sup>127,128</sup> the  
669 enzyme to the electrode. New electrochemical theory and models will benefit electrode structure  
670 design and further optimization<sup>126</sup>.

671 Protein films in PFE are typically prepared for and used to study one enzyme at a time. However, many  
672 interesting metabolic pathways, for example methanogenesis, contain enzyme cascades. The  
673 products of PFE, such as NAD(P)H, are high-value substrates for industrially relevant enzymes and  
674 biocatalytic reactions. Coupling multiple enzymes on a surface, or trapping them in small  
675 compartments on the electrode, will provide new opportunities in biotechnology<sup>129</sup> and to control  
676 points within a metabolic pathway<sup>130-132</sup>.

677 For PFE to find widespread applications in biosensing, it is necessary to use reproducible, cheap, and  
678 possibly single-use electrodes. Historically, most laboratories used home built WEs, although some  
679 electrodes suitable for PFE are now commercially available. This situation is expected to stimulate  
680 more research using PFE. Commercially available and affordable single-use electrodes, such as screen-  
681 printed electrodes, that support reproducible PFE would benefit applications in biosensing and  
682 diagnostics.

683 There are several classes of proteins that are difficult to study with PFE. The first is membrane  
684 proteins, which require detergents to accommodate their amphiphilic nature and prevent  
685 aggregation. However, detergent micelles in solution and around the protein can interfere with  
686 protein film formation. PFE is possible for membrane proteins with large extramembranous domains  
687 and relatively small transmembrane domains<sup>133 134</sup>, but is increasingly difficult for complex polytopic  
688 membrane proteins. Electrodes have been designed to accommodate membrane proteins within lipid  
689 membranes<sup>135</sup>, but imbedding in a lipid membrane influences the orientation of a membrane protein  
690 on an electrode surface. New methods, for instance with nanoparticles<sup>136</sup>, need to be explored to see  
691 how membrane proteins can be studied with PFE.

692 A second class of oxidoreductases that are difficult to study with PFE are those that have a ping-pong  
693 mechanism with active sites buried deep in the enzyme core. An example is glucose oxidase, where  
694 oxygen and glucose alternatively bind to an active site flavin adenine dinucleotide (FAD) in the centre  
695 of the protein. The relatively long distance between the FAD and protein surface means that direct  
696 electron transfer to the WE is strongly impaired and requires special considerations, such as  
697 attachment of gold nanoparticles at specific surface sites<sup>137</sup>. There are only a few examples of PFE  
698 used to study enzymes with radical intermediates, that undergo thiol-disulphide interconversion, that  
699 produce radical oxygen species or that produce radical nitrogen species<sup>138,139</sup>. Developing strategies  
700 to interface oxidoreductases with WEs will extend the number of redox proteins and processes that  
701 can be studied with PFE.

702 This manuscript has focussed on CV and CA. However, other techniques have contributed to the  
703 development of PFE, notably square-wave voltammetry, differential pulse voltammetry and  
704 electrochemical impedance spectroscopy<sup>62,140-142</sup>. Developments in large amplitude sinusoidal  
705 voltammetry or Fourier transform alternating current voltammetry have enabled differentiation of  
706 various components that contribute to voltametric currents, for instance, non-Faradaic versus  
707 Faradaic currents, or catalytic versus non-catalytic currents<sup>138,143,144</sup>. To widen the use of these  
708 techniques, they need to become available on commercial potentiostats, with freely accessible  
709 software for analysis.

710



## References:

- 713 1 Liu, J. *et al.* Metalloproteins containing cytochrome, iron-sulfur, or copper redox centers.  
714 *Chem Rev* **114**, 4366-4469 (2014). <https://doi.org:10.1021/cr400479b>
- 715 2 Lippard, S. J. & Berg, J. M. *Principles of Bioinorganic Chemistry*. (University Science Books,  
716 1994).
- 717 3 Moser, C. C., Keske, J. M., Warncke, K., Farid, R. S. & Dutton, P. L. Nature of biological  
718 electron transfer. *Nature* **355**, 796-802 (1992). <https://doi.org:10.1038/355796a0>
- 719 4 Armstrong, F. A., Evans, R. M. & Megarity, C. F. Protein film electrochemistry of iron-sulfur  
720 enzymes. *Meth Enzymol* **599**, 387-407 (2018). <https://doi.org:10.1016/bs.mie.2017.11.001>
- 721 5 Armstrong, F. A., Heering, H. A. & Hirst, J. Reactions of complex metalloproteins studied by  
722 protein-film voltammetry. *Chem Soc Rev* **26**, 169-179 (1997).  
723 <https://doi.org:10.1039/cs9972600169>
- 724 6 Armstrong, F. A. & Wilson, G. S. Recent developments in Faradaic bioelectrochemistry.  
725 *Electrochim Acta* **45**, 2623-2645 (2000). [https://doi.org:10.1016/S0013-4686\(00\)00342-X](https://doi.org:10.1016/S0013-4686(00)00342-X)
- 726 7 del Barrio, M. *et al.* Electrochemical investigations of hydrogenases and other enzymes that  
727 produce and use solar fuels. *Acc Chem Res* **51**, 769-777 (2018).  
728 <https://doi.org:10.1021/acs.accounts.7b00622>
- 729 8 Leger, C. & Bertrand, P. Direct electrochemistry of redox enzymes as a tool for mechanistic  
730 studies. *Chem Rev* **108**, 2379-2438 (2008). <https://doi.org:10.1021/cr0680742>
- 731 9 Hirst, J. Elucidating the mechanisms of coupled electron transfer and catalytic reactions by  
732 protein film voltammetry. *BBA-Bioenergetics* **1757**, 225-239 (2006).  
733 <https://doi.org:10.1016/j.bbabi.2006.04.002>
- 734 10 Gates, A. J. *et al.* The relationship between redox enzyme activity and electrochemical  
735 potential-cellular and mechanistic implications from protein film electrochemistry. *Phys*  
736 *Chem Chem Phys* **13**, 7720-7731 (2011). <https://doi.org:10.1039/c0cp02887h>
- 737 11 Campbell-Rance, D. S., Doan, T. T. & Leopold, M. C. Sweep, step, pulse, and frequency-based  
738 techniques applied to protein monolayer electrochemistry at nanoparticle interfaces. *J*  
739 *Electroanal Chem* **662**, 343-354 (2011). <https://doi.org:10.1016/j.jelechem.2011.09.005>
- 740 12 Armstrong, F. A., Butt, J. N., George, S. J., Hatchikian, E. C. & Thomson, A. J. Evidence for  
741 reversible multiple redox transformations of [3Fe-4S] clusters. *FEBS Lett* **259**, 15-18 (1989).  
742 [https://doi.org:10.1016/0014-5793\(89\)81483-8](https://doi.org:10.1016/0014-5793(89)81483-8)
- 743 13 Feng, Z. Q., Imabayashi, S., Kakiuchi, T. & Niki, K. Electroreflectance spectroscopic study of  
744 the electron-transfer rate of cytochrome *c* electrostatically immobilized on the omega-  
745 carboxyl alkanethiol monolayer modified gold electrode. *J Electroanal Chem* **394**, 149-154  
746 (1995). [https://doi.org:10.1016/0022-0728\(95\)04058-V](https://doi.org:10.1016/0022-0728(95)04058-V)
- 747 14 Willit, J. L. & Bowden, E. F. Determination of unimolecular electron-transfer rate constants  
748 for strongly adsorbed cytochrome *c* on tin oxide electrodes. *J Electroanal Chem* **221**, 265-274  
749 (1987). [https://doi.org:10.1016/0022-0728\(87\)80264-4](https://doi.org:10.1016/0022-0728(87)80264-4)
- 750 15 Bard, A. J. & Faulkner, L. R. *Electrochemical Methods. Fundamentals and Applications.*, (John  
751 Wiley & Sons Inc., 2000).
- 752 16 Compton, R. & Banks, C. *Understanding Voltammetry* Third Edition edn, (WSPC (Europe),  
753 2018).
- 754 17 Nelson, D. L. & Cox, M. M. *Lehninger Principles of Biochemistry*. (W. H. Freeman, 2021).
- 755 18 Colburn, A. W., Levey, K. J., O'Hare, D. & Macpherson, J. V. Lifting the lid on the potentiostat:  
756 a beginner's guide to understanding electrochemical circuitry and practical operation. *Phys*  
757 *Chem Chem Phys* **23**, 8100-8117 (2021). <https://doi.org:10.1039/d1cp00661d>
- 758 19 Caux, M. *et al.* PassStat, a simple but fast, precise and versatile open source potentiostat.  
759 *HardwareX* **11**, e00290 (2022). <https://doi.org:10.1016/j.ohx.2022.e00290>
- 760 20 Hirst, J. & Armstrong, F. A. Fast-scan cyclic voltammetry of protein films on pyrolytic graphite  
761 edge electrodes: Characteristics of electron exchange. *Anal Chem* **70**, 5062-5071 (1998).  
762 <https://doi.org:10.1021/ac980557l>

- 763 21 Jeuken, L. J. C., McEvoy, J. P. & Armstrong, F. A. Insights into gated electron-transfer kinetics  
764 at the electrode-protein interface: A square wave voltammetry study of the blue copper  
765 protein azurin. *J Phys Chem B* **106**, 2304-2313 (2002). <https://doi.org:10.1021/jp0134291>  
766 22 Hirst, J. *et al.* Kinetics and mechanism of redox-coupled, long-range proton transfer in an  
767 iron-sulfur protein. Investigation by fast-scan protein-film voltammetry. *J Am Chem Soc* **120**,  
768 7085-7094 (1998). <https://doi.org:10.1021/ja980380c>  
769 23 Heering, H. A., Mondal, M. S. & Armstrong, F. A. Using the pulsed nature of staircase cyclic  
770 voltammetry to determine interfacial electron-transfer rates of adsorbed species. *Anal Chem*  
771 **71**, 174-182 (1999). <https://doi.org:10.1021/ac980844p>  
772 24 Anantharaj, S. & Noda, S. iR drop correction in electrocatalysis: everything one needs to  
773 know! *J Mater Chem A* **10**, 9348-9354 (2022). <https://doi.org:10.1039/d2ta01393b>  
774 25 Kato, M., Zhang, J. Z., Paul, N. & Reisner, E. Protein film photoelectrochemistry of the water  
775 oxidation enzyme photosystem II. *Chem Soc Rev* **43**, 6485-6497 (2014).  
776 <https://doi.org:10.1039/c4cs00031e>  
777 26 Sensi, M. *et al.* Photoinhibition of FeFe hydrogenase. *ACS Catal* **7**, 7378-7387 (2017).  
778 <https://doi.org:10.1021/acscatal.7b02252>  
779 27 Murgida, D. H. In situ spectroelectrochemical investigations of electrode-confined electron-  
780 transferring proteins and redox enzymes. *ACS Omega* **6**, 3435-3446 (2021).  
781 <https://doi.org:10.1021/acsomega.0c05746>  
782 28 Jeuken, L. J. C. Structure and modification of electrode materials for protein  
783 electrochemistry. *Adv Biochem Eng Biotechnol* **158**, 43-73 (2017).  
784 [https://doi.org:10.1007/10\\_2015\\_5011](https://doi.org:10.1007/10_2015_5011)  
785 29 Sahin, S. & Milton, R. D. Evolving enzymatic electrochemistry with rare or unnatural amino  
786 acids. *Curr Opin Electrochem* **35**, 101102 (2022).  
787 <https://doi.org:10.1016/j.coelec.2022.101102>  
788 30 Campbell, W. H., Henig, J. & Plumere, N. Affinity binding via Zinc(II) for controlled orientation  
789 and electrochemistry of Histidine-tagged nitrate reductase in self-assembled monolayers.  
790 *Bioelectrochem* **93**, 46-50 (2013). <https://doi.org:10.1016/j.bioelechem.2012.07.002>  
791 31 Baffert, C. *et al.* Covalent attachment of FeFe hydrogenases to carbon electrodes for direct  
792 electron transfer. *Anal Chem* **84**, 7999-8005 (2012). <https://doi.org:10.1021/ac301812s>  
793 32 Holzinger, M., Cosnier, S. & Buzzetti, P. H. M. The versatility of pyrene and its derivatives on  
794 sp<sup>2</sup> carbon nanomaterials for bioelectrochemical applications. *Synth Met* **292** (2023).  
795 <https://doi.org:10.1016/j.synthmet.2022.117219>  
796 33 Mahouche-Chergui, S., Gam-Derouich, S., Mangeney, C. & Chehimi, M. M. Aryl diazonium  
797 salts: a new class of coupling agents for bonding polymers, biomacromolecules and  
798 nanoparticles to surfaces. *Chem Soc Rev* **40**, 4143-4166 (2011).  
799 <https://doi.org:10.1039/c0cs00179a>  
800 34 Love, J. C., Estroff, L. A., Kriebel, J. K., Nuzzo, R. G. & Whitesides, G. M. Self-assembled  
801 monolayers of thiolates on metals as a form of nanotechnology. *Chem Rev* **105**, 1103-1169  
802 (2005). <https://doi.org:10.1021/cr0300789>  
803 35 Yan, X. M., Tang, J., Tanner, D., Ulstrup, J. & Xiao, X. X. Direct electrochemical enzyme  
804 electron transfer on electrodes modified by self-assembled molecular monolayers. *Catalysts*  
805 **10** (2020). <https://doi.org:10.3390/catal10121458>  
806 36 Doan, T. T., Freeman, M. H., Schmidt, A. R., Nguyen, N. D. T. & Leopold, M. C. Synthesis,  
807 assembly, and characterization of monolayer protected gold nanoparticle films for protein  
808 monolayer electrochemistry. *JoVE*, e3441 (2011). <https://doi.org:10.3791/3441>  
809 37 Oviedo-Rouco, S. *et al.* Correlated electric field modulation of electron transfer parameters  
810 and the access to alternative conformations of multifunctional cytochrome c.  
811 *Bioelectrochem* **143**, 107956 (2022). <https://doi.org:10.1016/j.bioelechem.2021.107956>  
812 38 Mersch, D. *et al.* Wiring of Photosystem II to hydrogenase for photoelectrochemical water  
813 splitting. *J Am Chem Soc* **137**, 8541-8549 (2015). <https://doi.org:10.1021/jacs.5b03737>

- 814 39 Morlock, S., Subramanian, S. K., Zouni, A. & Lisdat, F. Closing the green gap of photosystem I  
815 with synthetic fluorophores for enhanced photocurrent generation in photobiocathodes.  
816 *Chem Sci* **14**, 1696-1708 (2023). <https://doi.org:10.1039/d2sc05324a>
- 817 40 Siritanaratkul, B. *et al.* Transfer of photosynthetic NADP(+)/NADPH recycling activity to a  
818 porous metal oxide for highly specific, electrochemically-driven organic synthesis. *Chem Sci*  
819 **8**, 4579-4586 (2017). <https://doi.org:10.1039/c7sc00850c>
- 820 41 Morlock, S., Subramanian, S. K., Zouni, A. & Lisdat, F. Bio-inorganic hybrid structures for  
821 direct electron transfer to photosystem I in photobioelectrodes. *Biosens Bioelectron* **214**,  
822 114495 (2022). <https://doi.org:10.1016/j.bios.2022.114495>
- 823 42 Fourmond, V. QSoas: a versatile software for data analysis. *Anal Chem* **88**, 5050-5052 (2016).  
824 <https://doi.org:10.1021/acs.analchem.6b00224>
- 825 43 Merrouch, M., Hadj-Said, J., Leger, C., Dementin, S. & Fourmond, V. Reliable estimation of  
826 the kinetic parameters of redox enzymes by taking into account mass transport towards  
827 rotating electrodes in protein film voltammetry experiments. *Electrochim Acta* **245**, 1059-  
828 1064 (2017). <https://doi.org:10.1016/j.electacta.2017.03.114>
- 829 44 Fourmond, V. & Leger, C. Modelling the voltammetry of adsorbed enzymes and molecular  
830 catalysts. *Curr Opin Electrochem* **1**, 110-120 (2017).  
831 <https://doi.org:10.1016/j.coelec.2016.11.002>
- 832 45 Heering, H. A., Wiertz, F. G. M., Dekker, C. & de Vries, S. Direct immobilization of native  
833 yeast Iso-1 cytochrome *c* on bare gold: Fast electron relay to redox enzymes and zeptomole  
834 protein-film voltammetry. *J Am Chem Soc* **126**, 11103-11112 (2004).  
835 <https://doi.org:10.1021/ja046737w>
- 836 46 Wang, M. K., Zhao, F., Liu, Y. & Dong, S. J. Direct electrochemistry of microperoxidase at Pt  
837 microelectrodes modified with carbon nanotubes. *Biosens Bioelectron* **21**, 159-166 (2005).  
838 <https://doi.org:10.1016/j.bios.2004.08.012>
- 839 47 Lockwood, C. W. J. *et al.* Resolution of key roles for the distal pocket histidine in cytochrome  
840 *c* nitrite reductases. *J Am Chem Soc* **137**, 3059-3068 (2015).  
841 <https://doi.org:10.1021/ja512941j>
- 842 48 Marritt, S. J. *et al.* Spectroelectrochemical characterization of a pentaheme cytochrome in  
843 solution and as electrocatalytically active films on nanocrystalline metal-oxide electrodes. *J*  
844 *Am Chem Soc* **130**, 8588-8589 (2008). <https://doi.org:10.1021/ja802641a>
- 845 49 Reuillard, B. *et al.* High performance reduction of H<sub>2</sub>O<sub>2</sub> with an electron transport decaheme  
846 cytochrome on a porous ITO electrode. *J Am Chem Soc* **139**, 3324-3327 (2017).  
847 <https://doi.org:10.1021/jacs.6b12437>
- 848 50 Ash, P. A., Hidalgo, R. & Vincent, K. A. Protein film infrared electrochemistry demonstrated  
849 for study of H<sub>2</sub> oxidation by a [NiFe] hydrogenase. *JoVE*, e55858 (2017).  
850 <https://doi.org:10.3791/55858>
- 851 51 Chung, M. W. *et al.* Infrared spectroscopy coupled with protein film electrochemistry to  
852 study hydrogenase inhibition by pi-acid ligands. *J Biol Inorg Chem* **19**, S879-S879 (2014).
- 853 52 Kornienko, N. *et al.* Advancing techniques for investigating the enzyme-electrode interface.  
854 *Acc Chem Res* **52**, 1439-1448 (2019). <https://doi.org:10.1021/acs.accounts.9b00087>
- 855 53 McEvoy, J. P. & Armstrong, F. A. Protein film cryovoltammetry: demonstrations with a 7Fe  
856 ([3Fe-4S]+[4Fe-4S]) ferredoxin. *Chem Commun*, 1635-1636 (1999).  
857 <https://doi.org:10.1039/a903222c>
- 858 54 Kornienko, N. *et al.* Oxygenic photoreactivity in Photosystem II studied by rotating ring disk  
859 electrochemistry. *J Am Chem Soc* **140**, 17923-17931 (2018).  
860 <https://doi.org:10.1021/jacs.8b08784>
- 861 55 Fourmond, V. & Leger, C. Protein electrochemistry: questions and answers. *Adv Biochem Eng*  
862 *Biot* **158**, 1-41 (2017). [https://doi.org:10.1007/10\\_2015\\_5016](https://doi.org:10.1007/10_2015_5016)
- 863 56 Hartshorne, R. S. *et al.* Characterization of *Shewanella oneidensis* MtrC: a cell-surface  
864 decaheme cytochrome involved in respiratory electron transport to extracellular electron

- 865 acceptors. *J Biol Inorg Chem* **12**, 1083-1094 (2007). [https://doi.org/10.1007/s00775-007-](https://doi.org/10.1007/s00775-007-0278-y)  
866 [0278-y](https://doi.org/10.1007/s00775-007-0278-y)
- 867 57 van Wonderen, J. H., Burlat, B., Richardson, D. J., Cheesman, M. R. & Butt, J. N. The nitric  
868 oxide reductase activity of cytochrome c nitrite reductase from *Escherichia coli*. *J Biol Chem*  
869 **283**, 9587-9594 (2008). <https://doi.org/10.1074/jbc.M709090200>
- 870 58 Laviron, E. General expression of the linear potential sweep voltammogram in the case of  
871 diffusionless electrochemical systems. *J Electroanal Chem* **101**, 19-28 (1979).  
872 [https://doi.org/10.1016/S0022-0728\(79\)80075-3](https://doi.org/10.1016/S0022-0728(79)80075-3)
- 873 59 Plichon, V. & Laviron, E. Theoretical study of a two-step reversible electrochemical reaction  
874 associated with irreversible chemical reactions in thin layer linear potential sweep  
875 voltammetry. *J. Electroanal. Chem.* **71**, 143-156 (1976). [https://doi.org/10.1016/S0022-](https://doi.org/10.1016/S0022-0728(76)80030-7)  
876 [0728\(76\)80030-7](https://doi.org/10.1016/S0022-0728(76)80030-7)
- 877 60 Jenner, L. P. *et al.* Reaction of thiosulfate dehydrogenase with a substrate mimic induces  
878 dissociation of the cysteine heme ligand giving insights into the mechanism of oxidative  
879 catalysis. *J Am Chem Soc* (2022). <https://doi.org/10.1021/jacs.2c06062>
- 880 61 Maiocco, S. J., Arcinas, A. J., Booker, S. J. & Elliott, S. J. Parsing redox potentials of five  
881 ferredoxins found within *Thermotoga maritima*. *Protein Sci* **28**, 257-266 (2019).  
882 <https://doi.org/10.1002/pro.3547>
- 883 62 Zhu, W. *et al.* Structural properties and catalytic implications of the SPASM domain iron-  
884 sulfur clusters in *Methylobacterium extorquens* PqqE. *J Am Chem Soc* **142**, 12620-12634 (2020).  
885 <https://doi.org/10.1021/jacs.0c02044>
- 886 63 Rizzolo, K. *et al.* A widely distributed diheme enzyme from *Burkholderia* that displays an  
887 atypically stable bis-Fe(IV) state. *Nat Commun* **10**, 1101 (2019).  
888 <https://doi.org/10.1038/s41467-019-09020-4>
- 889 64 Walker, L. M., Kincannon, W. M., Bandarian, V. & Elliott, S. J. Deconvoluting the reduction  
890 potentials for the three [4Fe-4S] clusters in an adoMet radical SCIFF maturase. *Biochemistry*  
891 **57**, 6050-6053 (2018). <https://doi.org/10.1021/acs.biochem.8b00846>
- 892 65 Armstrong, F. A. *et al.* Fast, long-range electron-transfer reactions of a 'blue' copper protein  
893 coupled non-covalently to an electrode through a stilbenyl thiolate monolayer. *Chem*  
894 *Commun*, 316-317 (2004). <https://doi.org/10.1039/b312936e>
- 895 66 Zitare, U. A. *et al.* The role of molecular crowding in long-range metalloprotein electron  
896 transfer: Dissection into site- and scaffold-specific contributions. *Electrochim Acta* **294**, 117-  
897 125 (2019). <https://doi.org/10.1016/j.electacta.2018.10.069>
- 898 67 Gulaboski, R., Kokoskarova, P. & Mitrev, S. Theoretical aspects of several successive two-step  
899 redox mechanisms in protein-film cyclic staircase voltammetry. *Electrochim Acta* **69**, 86-96  
900 (2012). <https://doi.org/10.1016/j.electacta.2012.02.086>
- 901 68 Shen, B. H. *et al.* *Azotobacter vinelandii* ferredoxin I. Aspartate-15 facilitates proton transfer  
902 to the reduced [3Fe-4S] cluster. *J Biol Chem* **268**, 25928-25939 (1993).  
903 [https://doi.org/10.1016/S0021-9258\(19\)74476-7](https://doi.org/10.1016/S0021-9258(19)74476-7)
- 904 69 Butt, J. N. *et al.* Voltammetric characterization of rapid and reversible binding of an  
905 exogenous thiolate ligand at a [4Fe-4S] cluster in Ferredoxin III from *Desulfovibrio africanus*.  
906 *J Am Chem Soc* **115**, 1413-1421 (1993). <https://doi.org/10.1021/ja00057a026>
- 907 70 Hirst, J., Jameson, G. N. L., Allen, J. W. A. & Armstrong, F. A. Very rapid, cooperative two-  
908 electron/two-proton redox reactions of [3Fe-4S] clusters: Detection and analysis by protein-  
909 film voltammetry. *J Am Chem Soc* **120**, 11994-11999 (1998).  
910 <https://doi.org/10.1021/ja981693a>
- 911 71 Camba, R. *et al.* Mechanisms of redox-coupled proton transfer in proteins: Role of the  
912 proximal proline in reactions of the [3Fe-4S] cluster in *Azotobacter vinelandii* ferredoxin I.  
913 *Biochemistry* **42**, 10589-10599 (2003). <https://doi.org/10.1021/bi035021v>
- 914 72 Steensma, E., Heering, H. A., Hagen, W. R. & vanMierlo, C. P. M. Redox properties of wild-  
915 type, Cys69Ala, and Cys69Ser *Azotobacter vinelandii* flavodoxin II as measured by cyclic

- 916 voltammetry and EPR spectroscopy. *Eur J Biochem* **235**, 167-172 (1996).  
917 <https://doi.org:10.1111/j.1432-1033.1996.00167.x>
- 918 73 Butt, J. N., Fawcett, S. E. J., Breton, J., Thomson, A. J. & Armstrong, F. A. Electrochemical  
919 potential and pH dependences of [3Fe-4S] $\leftrightarrow$ [M3Fe-4S] cluster transformations (M = Fe, Zn,  
920 Co, and Cd) in ferredoxin III from *Desulfovibrio africanus* and detection of a cluster with M =  
921 Pb. *J Am Chem Soc* **119**, 9729-9737 (1997). <https://doi.org:10.1021/ja971403a>
- 922 74 Butt, J. N., Niles, J., Armstrong, F. A., Breton, J. & Thomson, A. J. Formation and properties of  
923 a stable high-potential copper-iron-sulfur cluster in a ferredoxin. *Nat Struct Biol* **1**, 427-433  
924 (1994). <https://doi.org:10.1038/nsb0794-427>
- 925 75 Heering, H. A., Hirst, J. & Armstrong, F. A. Interpreting the catalytic voltammetry of  
926 electroactive enzymes adsorbed on electrodes. *J Phys Chem B* **102**, 6889-6902 (1998).  
927 <https://doi.org:10.1021/jp981023r>
- 928 76 Heering, H. A., Weiner, J. H. & Armstrong, F. A. Direct detection and measurement of  
929 electron relays in a multicentered enzyme: voltammetry of electrode-surface films of *E. coli*  
930 fumarate reductase, an iron-sulfur flavoprotein. *J Am Chem Soc* **119**, 11628-11638 (1997).  
931 <https://doi.org:10.1021/ja972324z>
- 932 77 Leger, C., Jones, A. K., Albracht, S. P. J. & Armstrong, F. A. Effect of a dispersion of interfacial  
933 electron transfer rates on steady state catalytic electron transport in [NiFe]-hydrogenase  
934 and other enzymes. *J Phys Chem B* **106**, 13058-13063 (2002).  
935 <https://doi.org:10.1021/jp0265687>
- 936 78 Sucheta, A., Cammack, R., Weiner, J. & Armstrong, F. A. Reversible electrochemistry of  
937 fumarate reductase immobilized on an electrode surface - direct voltammetric observations  
938 of redox centers and their participation in rapid catalytic electron-transport. *Biochemistry*  
939 **32**, 5455-5465 (1993). <https://doi.org:10.1021/bi00071a023>
- 940 79 Angove, H. C., Cole, J. A., Richardson, D. J. & Butt, J. N. Protein film voltammetry reveals  
941 distinctive fingerprints of nitrite and hydroxylamine reduction by a cytochrome c nitrite  
942 reductase. *J Biol Chem* **277**, 23374-23381 (2002). <https://doi.org:10.1074/jbc.M200495200>
- 943 80 Jones, A. K., Sillery, E., Albracht, S. P. J. & Armstrong, F. A. Direct comparison of the  
944 electrocatalytic oxidation of hydrogen by an enzyme and a platinum catalyst. *Chem*  
945 *Commun*, 866-867 (2002). <https://doi.org:10.1039/b201337a>
- 946 81 Armstrong, F. A. *et al.* Electrocatalytic reduction of hydrogen-peroxide at a stationary  
947 pyrolytic-graphite electrode surface in the presence of cytochrome c peroxidase - a  
948 description based on a microelectrode array model for adsorbed enzyme molecules. *Analyst*  
949 **118**, 973-978 (1993). <https://doi.org:10.1039/an9931800973>
- 950 82 Hoeben, F. J. M. *et al.* Polymyxin-coated Au and carbon nanotube electrodes for stable  
951 [NiFe]-hydrogenase film voltammetry. *Langmuir* **24**, 5925-5931 (2008).  
952 <https://doi.org:10.1021/la703984z>
- 953 83 Armstrong, F. A. Recent developments in dynamic electrochemical studies of adsorbed  
954 enzymes and their active sites. *Curr Opin Chem Biol* **9**, 110-117 (2005).  
955 <https://doi.org:10.1016/j.cbpa.2005.02.011>
- 956 84 Leger, C. *et al.* Enzyme electrokinetics: Energetics of succinate oxidation by fumarate  
957 reductase and succinate dehydrogenase. *Biochemistry* **40**, 11234-11245 (2001).  
958 <https://doi.org:10.1021/bi010889b>
- 959 85 Anderson, L. J., Richardson, D. J. & Butt, J. N. Catalytic protein film voltammetry from a  
960 respiratory nitrate reductase provides evidence for complex electrochemical modulation of  
961 enzyme activity. *Biochemistry* **40**, 11294-11307 (2001). <https://doi.org:10.1021/bi002706b>
- 962 86 Fourmond, V. *et al.* Correcting for electrocatalyst desorption and inactivation in  
963 chronoamperometry experiments. *Anal Chem* **81**, 2962-2968 (2009).  
964 <https://doi.org:10.1021/ac802570z>
- 965 87 Gwyer, J. D., Richardson, D. J. & Butt, J. N. Resolving complexity in the interactions of redox  
966 enzymes and their inhibitors: Contrasting mechanisms for the inhibition of a cytochrome c

967 nitrite reductase revealed by protein film voltammetry. *Biochemistry* **43**, 15086-15094  
968 (2004). <https://doi.org:10.1021/bi049085x>

969 88 Fourmond, V., Infossi, P., Giudici-Orticoni, M. T., Bertrand, P. & Leger, C. "Two-step"  
970 chronoamperometric method for studying the anaerobic inactivation of an oxygen tolerant  
971 NiFe hydrogenase. *J Am Chem Soc* **132**, 4848-4857 (2010). <https://doi.org:10.1021/ja910685j>

972 89 Leger, C., Dementin, S., Bertrand, P., Rousset, M. & Guigliarelli, B. Inhibition and aerobic  
973 inactivation kinetics of *Desulfovibrio fructosovorans* NiFe hydrogenase studied by protein  
974 film voltammetry. *J Am Chem Soc* **126**, 12162-12172 (2004).  
975 <https://doi.org:10.1021/ja046548d>

976 90 Leroux, F. *et al.* Experimental approaches to kinetics of gas diffusion in hydrogenase. *P Natl*  
977 *Acad Sci USA* **105**, 11188-11193 (2008). <https://doi.org:10.1073/pnas.0803689105>

978 91 Fourmond, V., Plumere, N. & Leger, C. Reversible catalysis. *Nat Rev Chem* **5**, 348-360 (2021).  
979 <https://doi.org:10.1038/s41570-021-00268-3>

980 92 Fourmond, V., Wiedner, E. S., Shaw, W. J. & Leger, C. Understanding and design of  
981 bidirectional and reversible catalysts of multielectron, multistep reactions. *J Am Chem Soc*  
982 **141**, 11269-11285 (2019). <https://doi.org:10.1021/jacs.9b04854>

983 93 Armstrong, F. A. & Hirst, J. Reversibility and efficiency in electrocatalytic energy conversion  
984 and lessons from enzymes. *P Natl Acad Sci USA* **108**, 14049-14054 (2011).  
985 <https://doi.org:10.1073/pnas.1103697108>

986 94 Kurth, J. M., Dahl, C. & Butt, J. N. Catalytic protein film electrochemistry provides a direct  
987 measure of the tetrathionate/thiosulfate reduction potential. *J Am Chem Soc* **137**, 13232-  
988 13235 (2015). <https://doi.org:10.1021/jacs.5b08291>

989 95 Wu, Y. H. & Hu, S. S. Biosensors based on direct electron transfer in redox proteins.  
990 *Microchim Acta* **159**, 1-17 (2007). <https://doi.org:10.1007/s00604-007-0749-4>

991 96 Das, P., Das, M., Chinnadayyala, S. R., Singha, I. M. & Goswami, P. Recent advances on  
992 developing 3rd generation enzyme electrode for biosensor applications. *Biosens Bioelectron*  
993 **79**, 386-397 (2016). <https://doi.org:10.1016/j.bios.2015.12.055>

994 97 Zuccarello, L., Barbosa, C., Todorovic, S. & Silveira, C. M. Electrocatalysis by heme enzymes-  
995 applications in biosensing. *Catalysts* **11** (2021). <https://doi.org:10.3390/catal11020218>

996 98 Gulaboski, R., Mirceski, V., Bogeski, I. & Hoth, M. Protein film voltammetry: electrochemical  
997 enzymatic spectroscopy. A review on recent progress. *J Solid State Electrochem* **16**, 2315-  
998 2328 (2012). <https://doi.org:10.1007/s10008-011-1397-5>

999 99 Ronkainen, N. J., Halsall, H. B. & Heineman, W. R. Electrochemical biosensors. *Chem Soc Rev*  
1000 **39**, 1747-1763 (2010). <https://doi.org:10.1039/b714449k>

1001 100 Sassolas, A., Blum, L. J. & Leca-Bouvier, B. D. Immobilization strategies to develop enzymatic  
1002 biosensors. *Biotechnol Adv* **30**, 489-511 (2012).  
1003 <https://doi.org:10.1016/j.biotechadv.2011.09.003>

1004 101 Datta, S., Christena, L. R. & Rajaram, Y. R. S. Enzyme immobilization: an overview on  
1005 techniques and support materials. *3 Biotech* **3**, 1-9 (2013). <https://doi.org:10.1007/s13205-012-0071-7>

1006 102 Bollella, P. & Katz, E. Enzyme-based biosensors: tackling electron transfer issues. *Sensors* **20**  
1007 (2020). <https://doi.org:10.3390/s20123517>

1008 103 Tan, T. C. *et al.* Structural basis for cellobiose dehydrogenase action during oxidative  
1009 cellulose degradation. *Nat Commun* **6** (2015). <https://doi.org:10.1038/ncomms8542>

1010 104 Tavahodi, M. *et al.* Direct electron transfer of cellobiose dehydrogenase on positively  
1011 charged polyethyleneimine gold nanoparticles. *ChemPlusChem* **82**, 546-552 (2017).  
1012 <https://doi.org:10.1002/cplu.201600453>

1013 105 Chen, H. *et al.* Fundamentals, applications, and future directions of bioelectrocatalysis. *Chem*  
1014 *Rev* **120**, 12903-12993 (2020). <https://doi.org:10.1021/acs.chemrev.0c00472>

1015 106 Xiao, X. X. *et al.* Tackling the challenges of enzymatic (bio)fuel cells. *Chem Rev* **119**, 9509-  
1016 9558 (2019). <https://doi.org:10.1021/acs.chemrev.9b00115>

1017



- 1018 107 Noll, T. & Noll, G. Strategies for "wiring" redox-active proteins to electrodes and applications  
1019 in biosensors, biofuel cells, and nanotechnology. *Chem Soc Rev* **40**, 3564-3576 (2011).  
1020 <https://doi.org:10.1039/c1cs15030h>
- 1021 108 Zhang, J. Z. & Reisner, E. Advancing photosystem II photoelectrochemistry for semi-artificial  
1022 photosynthesis. *Nat Rev Chem* **4**, 6-21 (2020). <https://doi.org:10.1038/s41570-019-0149-4>
- 1023 109 Terasaki, N. *et al.* Photocurrent generation properties of Histag-photosystem II immobilized  
1024 on nanostructured gold electrode. *Thin Solid Films* **516**, 2553-2557 (2008).  
1025 <https://doi.org:10.1016/j.tsf.2007.04.127>
- 1026 110 Kato, M., Cardona, T., Rutherford, A. W. & Reisner, E. Covalent immobilization of oriented  
1027 Photosystem II on a nanostructured electrode for solar water oxidation. *J Am Chem Soc* **135**,  
1028 10610-10613 (2013). <https://doi.org:10.1021/ja404699h>
- 1029 111 Jones, A. K., Camba, R., Reid, G. A., Chapman, S. K. & Armstrong, F. A. Interruption and time-  
1030 resolution of catalysis by a flavoenzyme using fast scan protein film voltammetry. *J Am Chem*  
1031 *Soc* **122**, 6494-6495 (2000). <https://doi.org:10.1021/ja000848n>
- 1032 112 Orain, C. *et al.* Electrochemical measurements of the kinetics of inhibition of two FeFe  
1033 Hydrogenases by O<sub>2</sub> demonstrate that the reaction is partly reversible. *J Am Chem Soc* **137**,  
1034 12580-12587 (2015). <https://doi.org:10.1021/jacs.5b06934>
- 1035 113 Field, S. J. *et al.* Reductive activation of nitrate reductases. *Dalton Trans*, 3580-3586 (2005).  
1036 <https://doi.org:10.1039/b505530j>
- 1037 114 Liebgott, P. P. *et al.* Relating diffusion along the substrate tunnel and oxygen sensitivity in  
1038 hydrogenase. *Nat Chem Biol* **6**, 63-70 (2010). <https://doi.org:10.1038/Nchembio.276>
- 1039 115 Wang, P. H. & Blumberger, J. Mechanistic insight into the blocking of CO diffusion in [NiFe]-  
1040 hydrogenase mutants through multiscale simulation. *P Natl Acad Sci USA* **109**, 6399-6404  
1041 (2012). <https://doi.org:10.1073/pnas.1121176109>
- 1042 116 Heering, H. A. & Hagen, W. R. Complex electrochemistry of flavodoxin at carbon-based  
1043 electrodes: Results from a combination of direct electron transfer, flavin-mediated electron  
1044 transfer and comproportionation. *J Electroanal Chem* **404**, 249-260 (1996).  
1045 [https://doi.org:10.1016/0022-0728\(95\)04248-2](https://doi.org:10.1016/0022-0728(95)04248-2)
- 1046 117 Hwang, E. T. *et al.* Exploring step-by-step assembly of nanoparticle: cytochrome biohybrid  
1047 photoanodes. *ChemElectroChem* **4**, 1959-1968 (2017).  
1048 <https://doi.org:10.1002/celec.201700030>
- 1049 118 Badiani, V. M. *et al.* Elucidating film loss and the role of hydrogen bonding of adsorbed redox  
1050 enzymes by electrochemical quartz crystal microbalance analysis. *ACS Catal* **12**, 1886-1897  
1051 (2022). <https://doi.org:10.1021/acscatal.1c04317>
- 1052 119 Beulen, M. W. J., Kastenbergh, M. I., van Veggel, F. C. J. M. & Reinhoudt, D. N. Electrochemical  
1053 stability of self-assembled monolayers on gold. *Langmuir* **14**, 7463-7467 (1998).  
1054 <https://doi.org:10.1021/la981031z>
- 1055 120 Ramos, N. C., Medlin, J. W. & Holewinski, A. Electrochemical stability of thiolate self-  
1056 assembled monolayers on Au, Pt, and Cu. *ACS Appl Mater Interfaces* **15**, 14470-14480  
1057 (2023). <https://doi.org:10.1021/acsami.3c01224>
- 1058 121 Milton, R. D. & Minteer, S. D. Direct enzymatic bioelectrocatalysis: differentiating between  
1059 myth and reality. *J R Soc Interface* **14**, 20170253 (2017).  
1060 <https://doi.org:10.1098/rsif.2017.0253>
- 1061 122 Ash, P. A., Kendall-Price, S. E. T. & Vincent, K. A. Unifying activity, structure, and  
1062 spectroscopy of [NiFe] hydrogenases: combining techniques to clarify mechanistic  
1063 understanding. *Acc Chem Res* **52**, 3120-3131 (2019).  
1064 <https://doi.org:10.1021/acs.accounts.9b00293>
- 1065 123 Abdiaziz, K., Salvadori, E., Sokol, K. P., Reisner, E. & Roessler, M. M. Protein film  
1066 electrochemical EPR spectroscopy as a technique to investigate redox reactions in  
1067 biomolecules. *Chem Commun* **55**, 8840-8843 (2019). <https://doi.org:10.1039/c9cc03212f>

- 1068 124 Chen, X. L. *et al.* 3D-printed hierarchical pillar array electrodes for high-performance semi-  
1069 artificial photosynthesis. *Nat Mater* **21**, 811-818 (2022). [https://doi.org:10.1038/s41563-](https://doi.org:10.1038/s41563-022-01205-5)  
1070 [022-01205-5](https://doi.org:10.1038/s41563-022-01205-5)
- 1071 125 Liu, Y. P. *et al.* Facile functionalization of carbon electrodes for efficient electroenzymatic  
1072 hydrogen production. *JACS Au* **3**, 124-130 (2023). <https://doi.org:10.1021/jacsau.2c00551>
- 1073 126 Moore, E. E. *et al.* Understanding the local chemical environment of bioelectrocatalysis. *P*  
1074 *Natl Acad Sci USA* **119**, e2114097119 (2022). <https://doi.org:10.1073/pnas.2114097119>
- 1075 127 Alonso-Lomillo, M. A. *et al.* Hydrogenase-coated carbon nanotubes for efficient H<sub>2</sub> oxidation.  
1076 *Nano Lett* **7**, 1603-1608 (2007). <https://doi.org:10.1021/nl070519u>
- 1077 128 Rudiger, O., Abad, J. M., Hatchikian, E. C., Fernandez, V. M. & De Lacey, A. L. Oriented  
1078 immobilization of *Desulfovibrio gigas* hydrogenase onto carbon electrodes by covalent  
1079 bonds for nonmediated oxidation of H<sub>2</sub>. *J Am Chem Soc* **127**, 16008-16009 (2005).  
1080 <https://doi.org:10.1021/ja0554312>
- 1081 129 Yarman, A. *et al.* Third generation ATP sensor with enzymatic analyte recycling. *Electroanal*  
1082 **26**, 2043-2048 (2014). <https://doi.org:10.1002/elan.201400231>
- 1083 130 Armstrong, F. A., Cheng, B. C., Herold, R. A., Megarity, C. F. & Siritanaratkul, B. From protein  
1084 film electrochemistry to nanoconfined enzyme cascades and the electrochemical leaf. *Chem*  
1085 *Rev* **123**, 5421-5458 (2023). <https://doi.org:10.1021/acs.chemrev.2c00397>
- 1086 131 Megarity, C. F., Weald, T. R. I., Heath, R. S., Turner, N. J. & Armstrong, F. A. A nanoconfined  
1087 four-enzyme cascade simultaneously driven by electrical and chemical energy, with built-in  
1088 rapid, confocal recycling of NADP(H) and ATP. *ACS Catal* **12**, 8811-8821 (2022).  
1089 <https://doi.org:10.1021/acscatal.2c00999>
- 1090 132 Lee, Y. S., Lim, K. & Minteer, S. D. Cascaded biocatalysis and bioelectrocatalysis: overview  
1091 and recent advances. *Annu Rev Phys Chem* **72**, 467-488 (2021).  
1092 <https://doi.org:10.1146/annurev-physchem-090519-050109>
- 1093 133 McMillan, D. G. G., Marritt, S. J., Butt, J. N. & Jeuken, L. J. C. Menaquinone-7 is specific  
1094 cofactor in tetraheme quinol dehydrogenase CymA. *J Biol Chem* **287**, 14215-14225 (2012).  
1095 <https://doi.org:10.1074/jbc.M112.348813>
- 1096 134 Gutierrez-Sanchez, C. *et al.* Oriented immobilization of a membrane-bound hydrogenase  
1097 onto an electrode for direct electron transfer. *Langmuir* **27**, 6449-6457 (2011).  
1098 <https://doi.org:10.1021/la200141t>
- 1099 135 Friedrich, M. G. *et al.* In situ monitoring of the catalytic activity of cytochrome c oxidase in a  
1100 biomimetic architecture. *Biophys J* **95**, 1500-1510 (2008).  
1101 <https://doi.org:10.1529/biophysj.107.122747>
- 1102 136 Meyer, T. *et al.* Evidence for distinct electron transfer processes in terminal oxidases from  
1103 different origin by means of protein film voltammetry. *J Am Chem Soc* **136**, 10854-10857  
1104 (2014). <https://doi.org:10.1021/ja505126v>
- 1105 137 Holland, J. T., Lau, C., Brozik, S., Atanassov, P. & Banta, S. Engineering of glucose oxidase for  
1106 direct electron transfer via site-specific gold nanoparticle conjugation. *J Am Chem Soc* **133**,  
1107 19262-19265 (2011). <https://doi.org:10.1021/ja2071237>
- 1108 138 Adamson, H. *et al.* Analysis of HypD disulfide redox chemistry via optimization of Fourier  
1109 Transformed ac voltammetric data. *Anal Chem* **89**, 1565-1573 (2017).  
1110 <https://doi.org:10.1021/acs.analchem.6b03589>
- 1111 139 Maiocco, S. J., Grove, T. L., Booker, S. J. & Elliott, S. J. Electrochemical resolution of the [4Fe-  
1112 4S] centers of the AdoMet radical enzyme BtrN: evidence of proton coupling and an unusual,  
1113 low-potential auxiliary cluster. *J Am Chem Soc* **137**, 8664-8667 (2015).  
1114 <https://doi.org:10.1021/jacs.5b03384>
- 1115 140 Jeuken, L. J. C., Jones, A. K., Chapman, S. K., Cecchini, G. & Armstrong, F. A. Electron-transfer  
1116 mechanisms through biological redox chains in multicenter enzymes. *J Am Chem Soc* **124**,  
1117 5702-5713 (2002). <https://doi.org:10.1021/ja012638w>

- 1118 141 Gulaboski, R. Theoretical contribution towards understanding specific behaviour of "simple"  
1119 protein-film reactions in square-wave voltammetry. *Electroanal* **31**, 545-553 (2019).  
1120 <https://doi.org:10.1002/elan.201800739>
- 1121 142 Pilz, F. H. & Kielb, P. Cyclic voltammetry, square wave voltammetry or electrochemical  
1122 impedance spectroscopy? Interrogating electrochemical approaches for the determination  
1123 of electron transfer rates of immobilized redox proteins *BBA Advances* **4** 100095 (2023).  
1124 <https://doi.org:10.1016/j.bbadv.2023.100095>
- 1125 143 Adamson, H., Bond, A. M. & Parkin, A. Probing biological redox chemistry with large  
1126 amplitude Fourier transformed ac voltammetry. *Chem Commun* **53**, 9519-9533 (2017).  
1127 <https://doi.org:10.1039/c7cc03870d>
- 1128 144 Bell, C. G., Anastassiou, C. A., O'Hare, D., Parker, K. H. & Siggers, J. H. Theoretical treatment  
1129 of high-frequency, large-amplitude ac voltammetry applied to ideal surface-confined redox  
1130 systems. *Electrochim Acta* **64**, 71-80 (2012). <https://doi.org:10.1016/j.electacta.2011.12.088>

1131

1132

1133 **HIGHLIGHTED REFERENCES:**

1134

1135 Leger, C. & Bertrand, P. Direct electrochemistry of redox enzymes as a tool for mechanistic studies.  
1136 *Chem Rev* 108, 2379-2438 (2008). <https://doi.org:10.1021/cr0680742>

1137 **This comprehensive review summarises several models developed to interpret the PFE of**  
1138 **adsorbed redox proteins and enzymes, it also explains how the models are used to analyse**  
1139 **experimental data.**

1140

1141 Colburn, A. W., Levey, K. J., O'Hare, D. & Macpherson, J. V. Lifting the lid on the potentiostat: a  
1142 beginner's guide to understanding electrochemical circuitry and practical operation. *Phys Chem*  
1143 *Chem Phys* 23, 8100-8117 (2021). <https://doi.org:10.1039/d1cp00661d>

1144 **An excellent tutorial review on the operation of potentiostats and problem-solving issues that can**  
1145 **arise with electrochemical measurements.**

1146

1147 Hirst, J. & Armstrong, F. A. Fast-scan cyclic voltammetry of protein films on pyrolytic graphite edge  
1148 electrodes: Characteristics of electron exchange. *Anal Chem* 70, 5062-5071 (1998).  
1149 <https://doi.org:10.1021/ac980557l>

1150

1151 **Rates of interfacial electron transfer are quantified for four different proteins, the resulting**  
1152 **models consider Marcus and Butler-Volmer descriptions of interfacial electron transfer and form**  
1153 **the foundations for many subsequent models of more complex behaviours.**

1154

1155

1156 Baffert, C. *et al.* Covalent attachment of FeFe hydrogenases to carbon electrodes for direct electron  
1157 transfer. *Anal Chem* 84, 7999-8005 (2012). <https://doi.org:10.1021/ac301812s>

1158 **An excellent introduction to the benefits and complexities of covalent attachment of enzymes to**  
1159 **electrodes for PFE.**

1160

1161 Mersch, D. *et al.* Wiring of Photosystem II to hydrogenase for photoelectrochemical water splitting. *J*  
1162 *Am Chem Soc* 137, 8541-8549 (2015). <https://doi.org:10.1021/jacs.5b03737>

1163 **This paper describes PFE using hierarchical inverse-opal ITO working electrodes prepared by a**  
1164 **method now used by many different research groups.**

1165

1166 Kornienko, N. *et al.* Oxygenic photoreactivity in Photosystem II studied by rotating ring disk  
1167 electrochemistry. *J Am Chem Soc* 140, 17923-17931 (2018). <https://doi.org:10.1021/jacs.8b08784>

1168 **An elegant example of the power of PFE to deconvolute complexity in enzyme mechanism that**  
1169 **benefits from the use of a rotating ring disk electrode.**

1170

1171

1172 Laviron, E. General expression of the linear potential sweep voltammogram in the case of  
1173 diffusionless electrochemical systems. *J Electroanal Chem* 101, 19-28 (1979).  
1174 [https://doi.org:10.1016/S0022-0728\(79\)80075-3](https://doi.org:10.1016/S0022-0728(79)80075-3)

1175 **This landmark paper derives equations for the non-catalytic voltammetry of adsorbed redox**  
1176 **centres and that are used ubiquitously in the analysis of PFE.**

1177

1178 Butt, J. N. *et al.* Voltammetric characterization of rapid and reversible binding of an exogenous  
1179 thiolate ligand at a [4Fe-4S] cluster in Ferredoxin III from *Desulfovibrio africanus*. *J Am Chem Soc* 115,  
1180 1413-1421 (1993). <https://doi.org:10.1021/ja00057a026>  
1181 **A comprehensive illustration of how PFE can detect and quantify chemical reactions coupled to**  
1182 **redox transitions (EC and CE reactions).**

1183  
1184

1185 Hirst, J., Jameson, G. N. L., Allen, J. W. A. & Armstrong, F. A. Very rapid, cooperative two-  
1186 electron/two-proton redox reactions of [3Fe-4S] clusters: Detection and analysis by protein-film  
1187 voltammetry. *J Am Chem Soc* 120, 11994-11999 (1998). <https://doi.org:10.1021/ja981693a>  
1188

1189 **An elegant account of the use of PFE to quantify the rates of redox-coupled proton (un)binding**  
1190 **events.**

1191

1192 Milton, R. D. & Minteer, S. D. Direct enzymatic bioelectrocatalysis: differentiating between myth and  
1193 reality. *J R Soc Interface* 14, 20170253 (2017). <https://doi.org:10.1098/rsif.2017.0253>  
1194

1195 **Some important control studies that need to be done to ensure PFE responses are not due to**  
1196 **artefacts such as dissociated co-factors are highlighted in the final section of this review article.**

1197  
1198

1199 Ash, P. A., Kendall-Price, S. E. T. & Vincent, K. A. Unifying activity, structure, and spectroscopy of  
1200 [NiFe] hydrogenases: combining techniques to clarify mechanistic understanding. *Acc Chem Res* 52,  
1201 3120-3131 (2019). <https://doi.org:10.1021/acs.accounts.9b00293>  
1202

1203 **An excellent review on the benefits of combining spectroscopy with PFE.**

1204  
1205

1206 Chen, X. L. *et al.* 3D-printed hierarchical pillar array electrodes for high-performance semi-artificial  
1207 photosynthesis. *Nat Mater* 21, 811-818 (2022). <https://doi.org:10.1038/s41563-022-01205-5>  
1208

1209 **Further progress in PFE will in part depend on improved electrode materials and this paper**  
1210 **describes an elegant printing technique to create (nano)structured electrodes.**

1211  
1212

1213 Liu, Y. P. *et al.* Facile functionalization of carbon electrodes for efficient electroenzymatic hydrogen  
1214 production. *JACS Au* 3, 124-130 (2023). <https://doi.org:10.1021/jacsau.2c00551>  
1215

1216 **Application of PFE in catalysis requires high current densities and this paper describes a relatively**  
1217 **easy way to achieve this with hydrogenases.**

1218  
1219

1220

1221 **Acknowledgments.**

1222 JNB and LJCJ thank Professor Fraser Armstrong for inspiring and guiding their introduction to PFE,  
1223 and the many students and colleagues with whom they have subsequently collaborated in applying  
1224 and developing the technique. They are grateful for long-term funding from UK Research Councils,  
1225 notably BBSRC most recently through grants BB/S000704/1 and BB/S002499/1. JAJB is funded by a  
1226 PhD studentship from the University of East Anglia and ASC by the UKRI Biotechnology and Biological  
1227 Sciences Research Council Norwich Research Park Biosciences Doctoral Training Partnership [Grant  
1228 number BB/T008717/1).

1229

1230

1231 **Competing Interests:**

1232 The authors declare no competing interests

1233

1234

1235 **FIGURE LEGENDS:**

1236

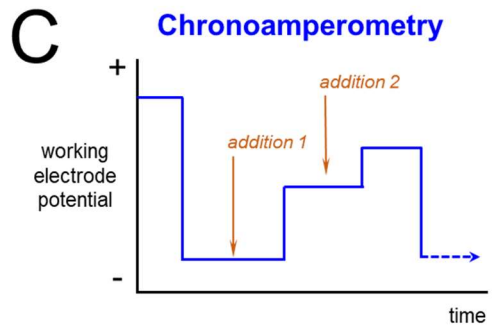
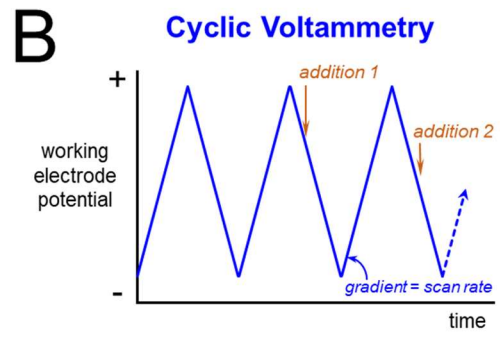
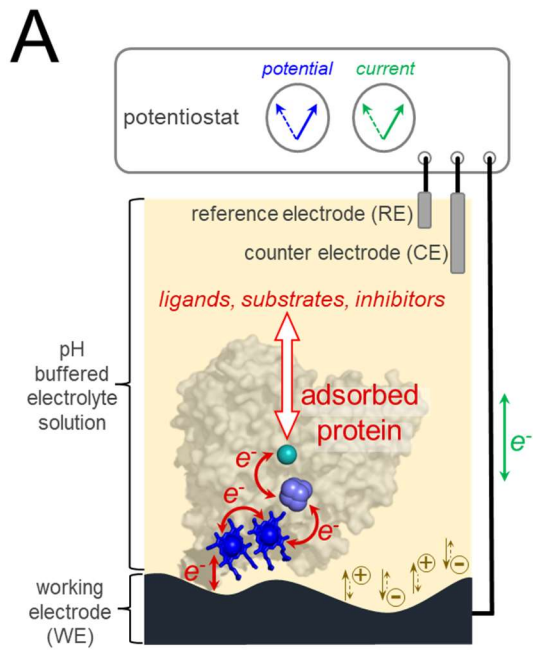
1237

1238 **Fig. 1 | Concept of protein film electrochemistry (PFE). A|** The protein of interest is adsorbed as a  
1239 (sub-)monolayer film on a working electrode (WE). Direct electron transfer occurs between the WE  
1240 and a redox cofactor terminating a chain of additional redox sites within the protein: heme (royal  
1241 blue), iron-sulphur cluster (navy) and Mo (teal) cofactors (PDB ID: 1OGY). The protein retains full  
1242 activity towards molecules and/or ions introduced to the surrounding electrolyte solution. The Mo  
1243 cofactor is the active site of this redox enzyme. The hemes and iron-sulphur cluster relay electrons  
1244 between the active site and the WE. A potentiostat applies defined and variable potential to the WE  
1245 while simultaneously measuring the flow of current through that electrode. The measured current has  
1246 two contributions: Faradaic current due to redox transformation in the protein (red arrows),  
1247 capacitance due to migration of electrolyte ions (brown arrows). **B|** The excitation profile applied  
1248 during cyclic voltammetry (CV) illustrating how scan rate is defined. **C|** An excitation profile for  
1249 chronoamperometry (CA). Brown arrows indicate that reactants can be introduced at desired times in  
1250 both CV (B) and CA (C).

1251

1252

1253





1255

1256

1257

1258

1259

1260

1261

1262

1263

1264

1265

1266

1267

1268

1269

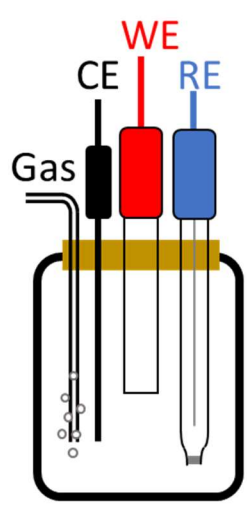
1270

1271

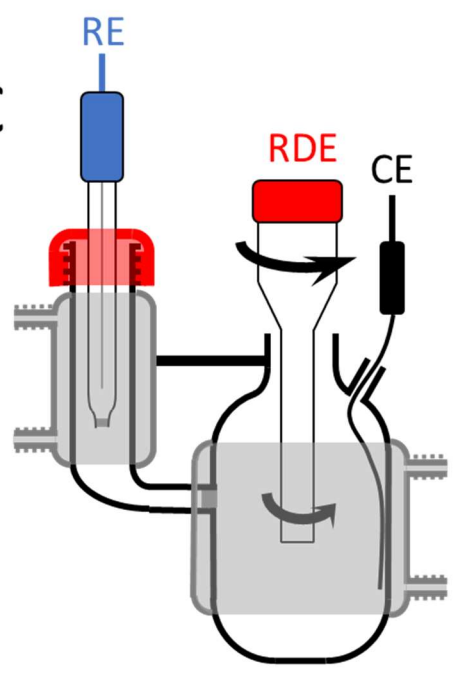
1272

**Fig. 2 | Schematics of electrochemical cells. (WE = working electrode; CE = counter electrode; RE = reference electrode).** **A** | A basic electrochemical cell such as can be purchased commercially for use with a rod-shaped WE. **B** | An optimised electrochemical cell for stationary electrochemistry with a rod-shaped WE. The main cell has a water jacket (grey) for temperature control. The RE is placed to the side of the main cell to enable separate temperature control. Leakage of RE solution (for instance saturated KCl solution) into the main cell is minimised by using a second junction (either a glass frit or a luggin capillary). The second junction is placed close to the WE to minimize solution resistance ( $R$ ) and hence potential drop ( $iR$  drop). **C** | Cell for use with a rotating disk electrode (RDE). The WE is a disk on the lower face of the rotated housing. The cell volume should be sufficiently large to preclude a significant drop of substrate concentration during measurement of redox catalysis. The CE and luggin tip are positioned to minimise turbulence. **D** | A basic electrochemical cell for working with a plate-shaped WE. If a transparent gold electrode is used — for example a <50 nm thick gold film on a glass slide — this cell can be combined with epi-fluorescent microscopy in an inverted microscope. Here, the glass cell is placed on top of the WE with an O-ring, which is not air-tight, and oxygen can slowly diffuse to the plate electrode from the side.

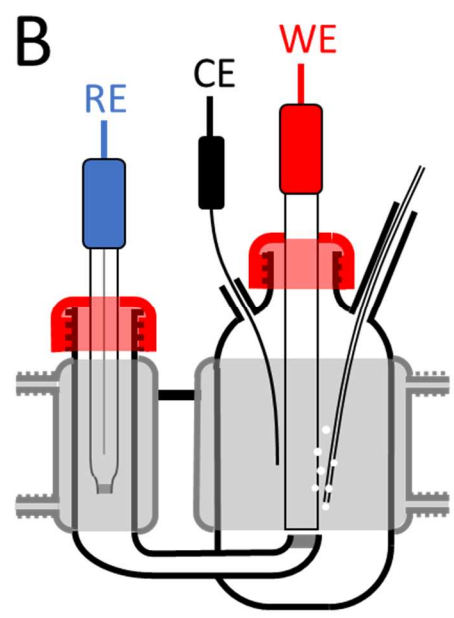
A



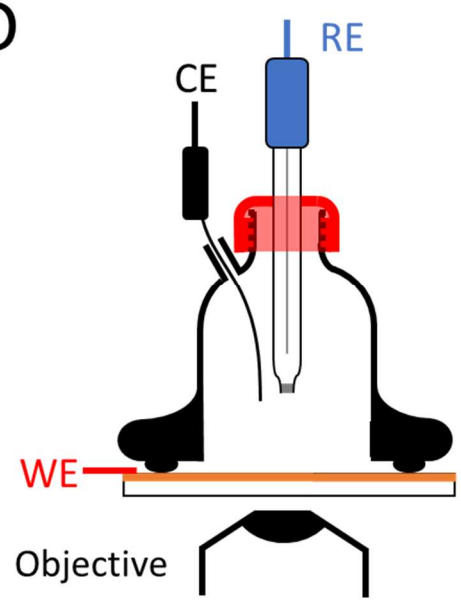
C



B



D

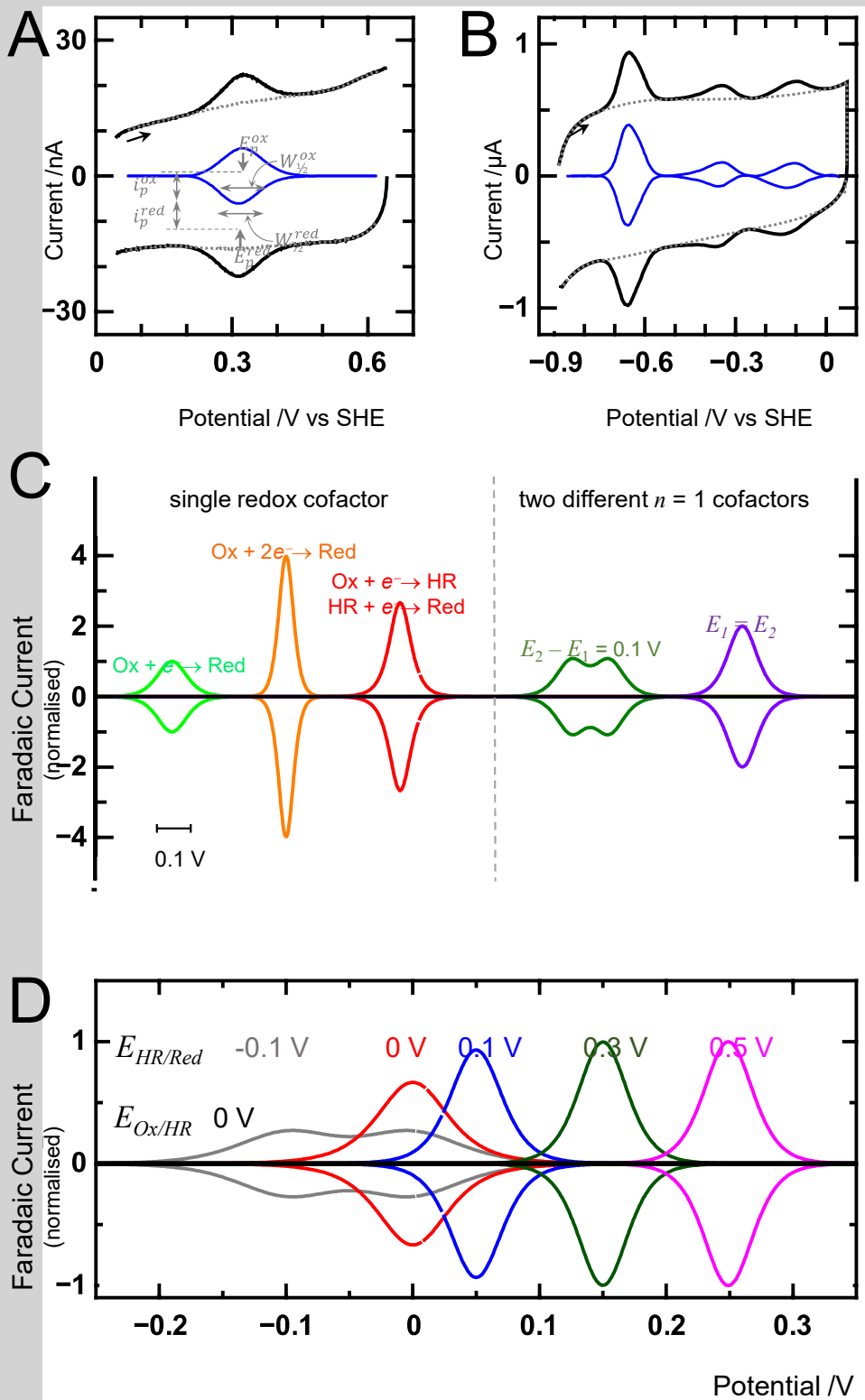


1273

1274 **Fig. 3 | Non-catalytic peaks in the cyclic voltammetry (CV) of adsorbed proteins.** **A** | Cyclic  
1275 voltammogram (black) of a protein with a single  $n = 1$  cofactor. Scan rate  $10 \text{ mV s}^{-1}$ , black arrow shows  
1276 the scan direction. Currents due to capacitance (grey dotted line) and Faradaic currents (blue) are also  
1277 shown. Peak potentials ( $E_p$ ), peak currents ( $i_p$ ) and half-height widths ( $W_{1/2}$ ) are indicated for the  
1278 oxidation (ox) and reduction (red) peaks. The peaks originate from a  $\text{Cu}^{2+/+}$  cofactor. **B** | Cyclic  
1279 voltammogram (black) of a protein with a single  $n = 2$  couple and two  $n = 1$  cofactors. Scan rate  $19 \text{ mV}$   
1280  $\text{s}^{-1}$ , black arrow indicates the scan direction. Charging currents (grey dotted line) and Faradaic currents  
1281 (blue) are also shown. The peaks originate from  $[\text{3Fe-4S}]^{1+/0}$ ,  $[\text{4Fe-4S}]^{2+/1+}$  and  $[\text{3Fe-4S}]^{0/2-}$  cofactors in  
1282 order of increasingly negative reduction potential. **C** | Examples of the Faradaic currents typically  
1283 produced by protein cofactors. For a single cofactor moving between oxidised (Ox) and reduced (Red)  
1284 states with  $n = 1$  (light green) and  $n = 2$  (orange). For a single cofactor where two sequential  $n = 1$   
1285 processes convert Ox to Red via a half-reduced (HR) state (red) and the reduction potentials for the  
1286 two half-reactions are equal. For two cofactors moving between their Ox and Red states in  $n = 1$   
1287 processes with  $E_2 - E_1 = 0.1 \text{ V}$  (dark green) and  $E_1 = E_2$  (purple). **D** | Faradaic currents that can be  
1288 produced by a single cofactor having two sequential  $n = 1$  process where conversion of Ox to Red via  
1289 a half-reduced (HR) state is described by  $E_{\text{Ox/HR}} = 0 \text{ V}$  and the value for  $E_{\text{HR/Red}}$  is as indicated. In  
1290 practice, measured non-catalytic peaks, for example panels A and B are typically broader and less  
1291 symmetrical about the potential axis than theory predicts.

1292

1293



1295

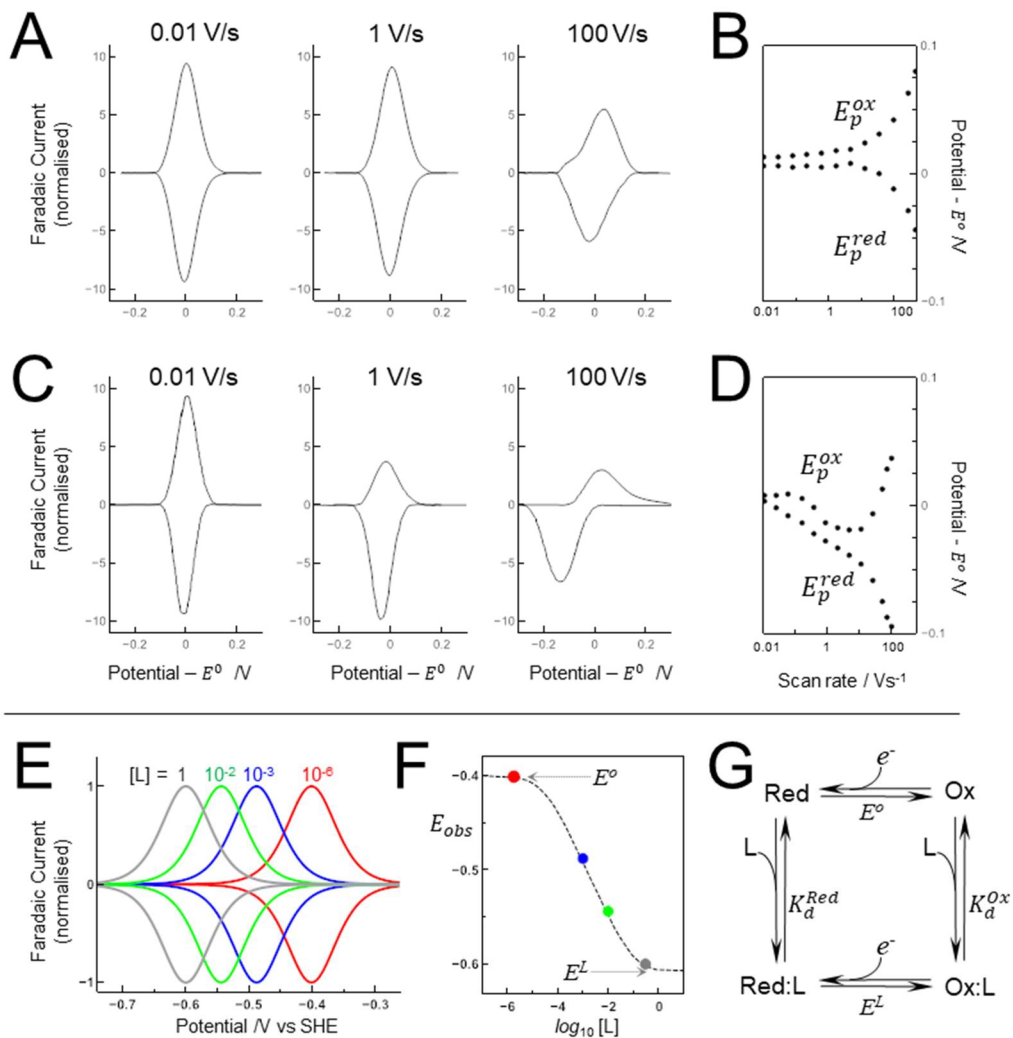
1296 **Fig. 4 | Trumpet plots and ligand binding and unbinding. A** | Faradaic currents from CV at the stated  
1297 scan rates illustrating behaviour typical for a reversible redox couple. **B** | Plot of peak potentials versus  
1298 scan rate on a log scale for the experiment in **A**. Symmetrical displacements of  $E_p^{ox}$  and  $E_p^{red}$  about  $E^o$   
1299 are indicative of reversible electron transfer uncomplicated by slow redox-driven chemistry. **C** |  
1300 Faradaic currents from CV at the stated scan rates illustrating behaviour indicative of fast reduction  
1301 followed by a slower, gated reoxidation due to ligand binding to the reduced protein. **D** | Plot of peak  
1302 potentials versus scan rate on a log scale for the experiment in **C**. At higher scan rates the  
1303 displacements of  $E_p^{ox}$  and  $E_p^{red}$  about  $E^o$  are not equal. **E** | Faradaic currents from CV at the stated  
1304 ligand (L) concentrations illustrating behaviour typical of ligand binding with greater affinity to an  
1305 oxidised than reduced cofactor. **F** | Variation of  $E^{obs}$  for the data in **E** fit to the behaviour predicted for  
1306 the dissociation constants  $K_d^{Ox} = 30 \mu\text{M}$ ,  $K_d^{Red} = 100 \text{mM}$  and a reduction potential ( $E^o$ ) of  $-0.4 \text{V}$  for  
1307 a non-ligated  $n = 1$  cofactor. **G** | Square-scheme illustrating ligand binding to an  $n = 1$  redox centre and  
1308 the corresponding thermodynamic parameters.

1309

1310

1311

1312

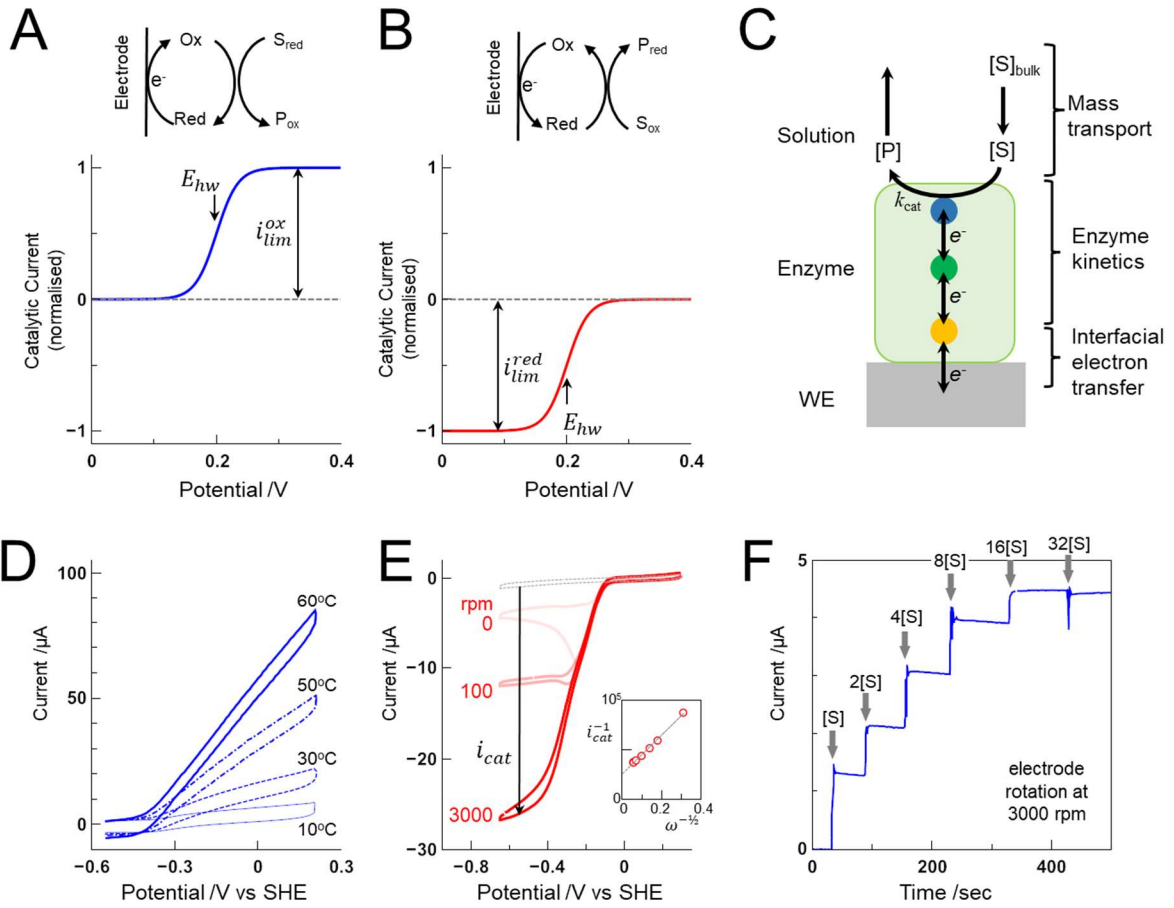


1313

1314 Fig. 5 | **Redox catalysis.** **A** | CV of adsorbed enzyme performing unidirectional oxidation of substrate  
1315 (S) to product (P). **B** | CV of adsorbed enzyme performing unidirectional substrate reduction. **C** |  
1316 Schematic illustration of processes that may determine the catalytic rate of an adsorbed enzyme:  
1317 substrate transport to the electrode, enzyme kinetics ( $k_{\text{cat}}$ ) and interfacial electron transfer. **D** | CV of  
1318 *A. vinosum* [NiFe] hydrogenase adsorbed on a PGE electrode. Temperature as indicated for 1 atmos.  
1319  $\text{H}_2$ , pH 7. Electrode rotation rate 2500 rpm. Scan rate  $1 \text{ V s}^{-1}$ . **E** | CV of *E. coli* cytochrome *c* nitrite  
1320 reductase adsorbed on a PGE electrode in  $130 \mu\text{M}$  nitrite (red). Electrode rotation at the indicated  
1321 rates. Scan rate  $30 \text{ mV s}^{-1}$ . CV in the absence of nitrite (grey). Arrow shows measurement of catalytic  
1322 current ( $i_{\text{cat}}$ ) at  $-550 \text{ mV}$  for the scan towards more negative potential at 3000 rpm. Inset: Koutecky-  
1323 Levich plot showing  $1/(i_{\text{cat}}$  measured at  $-550 \text{ mV})$  against  $1/(\text{angular velocity}, \omega)^{1/2}$ . **F** | CA for a redox  
1324 enzyme adsorbed on a PGE electrode rotated at 3000 rpm. Arrows indicate addition of substrate to  
1325 the electrochemical cell to give the indicated concentration.

1326

1327



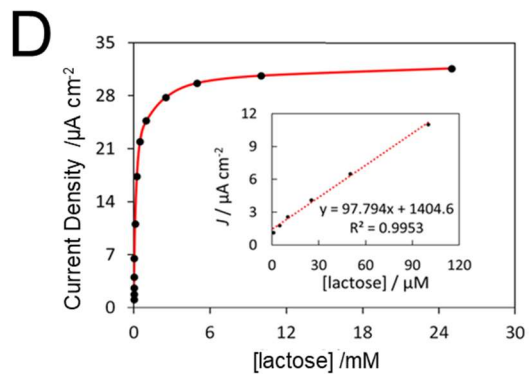
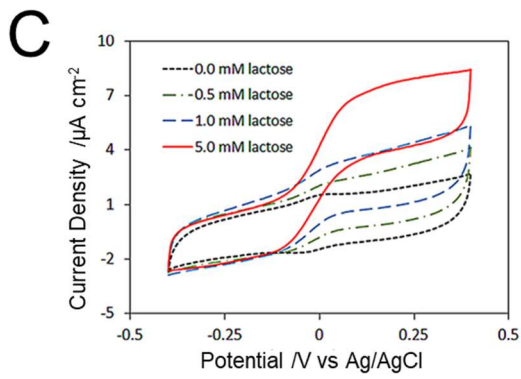
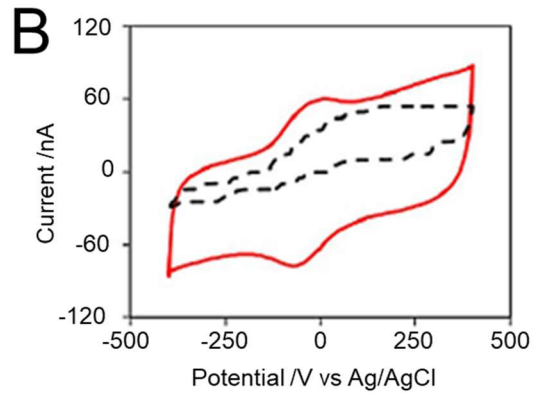
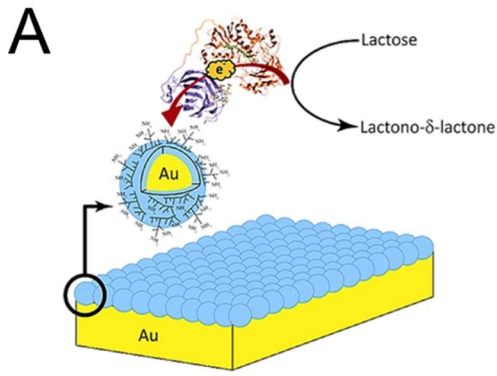


1329

1330

1331 **Fig. 6 | Biosensing. A** | Cartoon illustrating assembly and operation of a lactose biosensor using direct  
1332 electron transfer between AuNPs and the enzyme CDH. Blue: CYT domain. Red: DH domain. **B** | CV of  
1333 CDH adsorbed on PEI-AuNPs on a gold WE (red line) and directly on a gold WE (black line) in 5 mM  
1334 acetate, pH 4.5. Scan rate  $1 \text{ mV s}^{-1}$ . **C** | CV of *Ps*CDH electrostatically immobilized on PEI-AuNPs on a  
1335 gold WE for the indicated lactose concentrations in 5 mM acetate, pH 4.5. Scan rate  $1 \text{ mV s}^{-1}$ . **D** |  
1336 Variation of catalytic response with lactose concentration as defined by CA with the WE poised at +250  
1337 mV vs. Ag/AgCl (0.1 M KCl). Inset: the response in the low-micromolar range.

1338



1339

1340

1341

1342

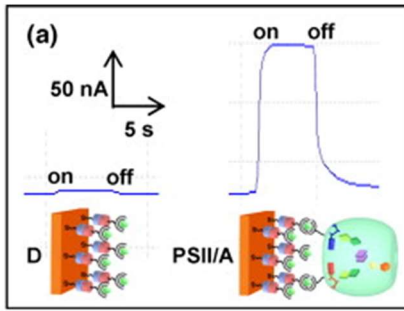
1343

1344

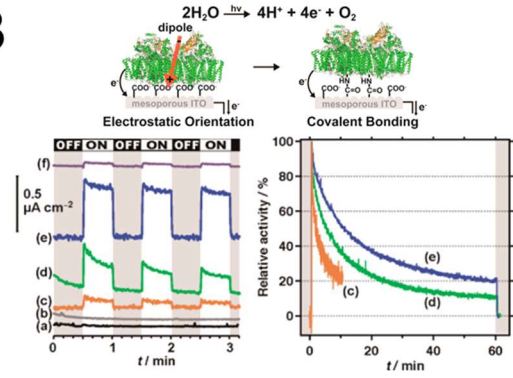
1345 Fig. 7 | **Photoreactivity. A** | CA of a gold WE coated with a SAM terminated by nickel-nitrilotriacetic  
1346 acid without (left) and with (right) polyhistidine tagged-PSII. WE held at 0.2 V vs. Ag/AgCl (sat. KCl). **B** |  
1347 Schematic of a mesoporous ITO WE coated with a carboxylate terminated SAM onto which PSII  
1348 spontaneously adsorbs (top left) and PSII covalently linked to the same electrode by carbodiimide with  
1349 N-hydroxy succinimide (top right). CA (bottom left) reporting catalytic currents during cycles of  
1350 irradiation by red-light for mesoporous ITO WEs coated with (a) carboxylate terminated SAM, (b)  
1351 carboxylate terminated SAM treated with carbodiimide and N-hydroxy succinimide, (c) PSII (d)  
1352 carboxylate terminated SAM and PSII, (e) carboxylate terminated SAM and PSII followed by exposure  
1353 to the coupling agents carbodiimide with N-hydroxy succinimide. (f) is a control experiment. CA  
1354 (bottom right) comparing the catalytic currents during continuous red-light irradiation for electrodes  
1355 (c–e). WEs poised at +0.5 V vs NHE. **C** | Cartoon of the RRDE setup for studying PSII photochemistry  
1356 (centre panel). CA revealing H<sub>2</sub>O oxidation by PSII at the glassy carbon disk electrode (0.5 V vs SHE)  
1357 and O<sub>2</sub> detection at the Pt ring electrode (-0.5 V vs SHE) (left panel). CA revealing reduction of O<sub>2</sub> by  
1358 PSII at the disk electrode with H<sub>2</sub>O<sub>2</sub> detected at the ring electrode. Electrode rotation at 400 rpm.

1359

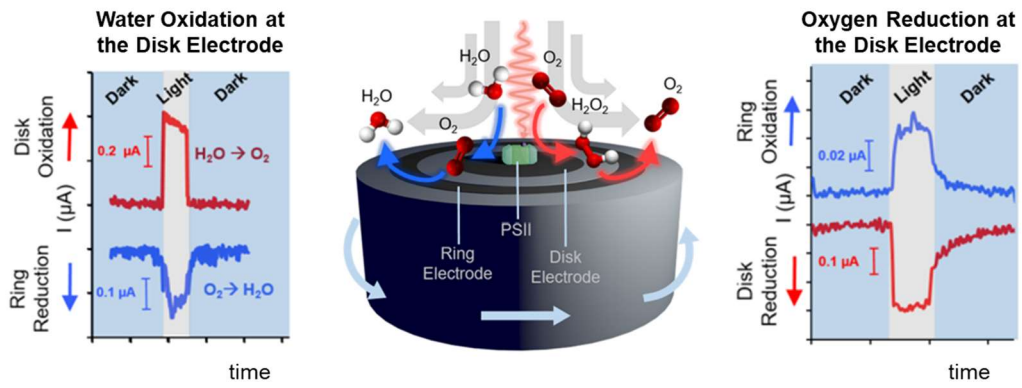
A



B



C



1360

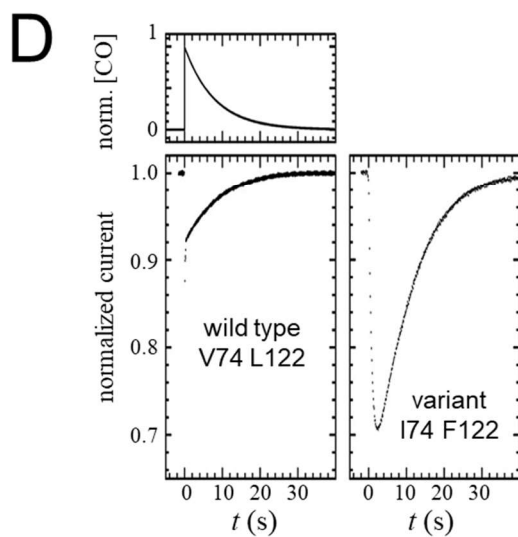
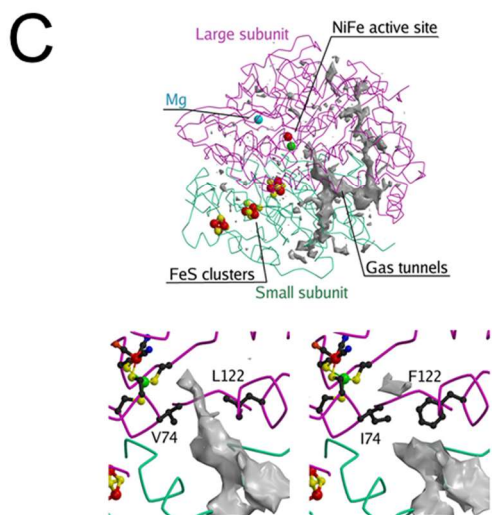
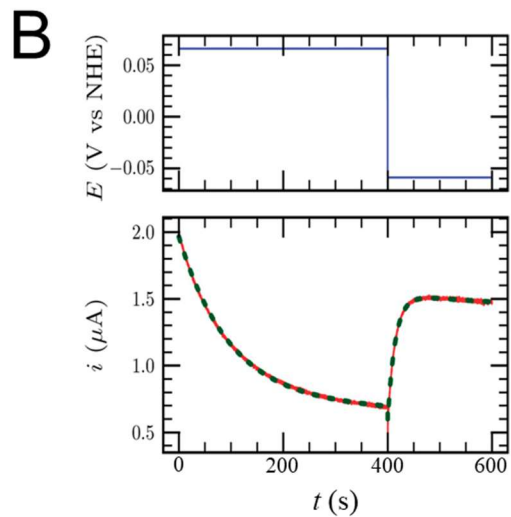
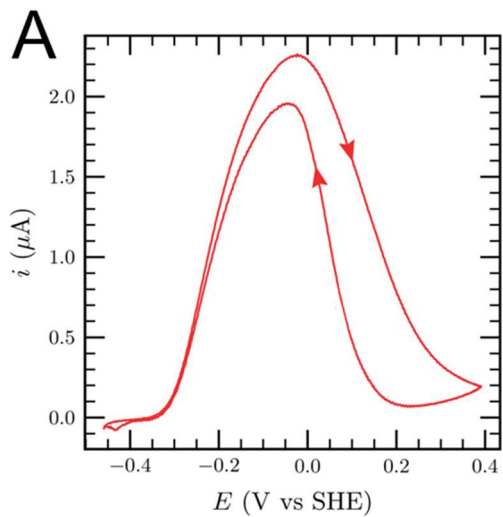
1361

1362

1363

1364 **Fig. 8 | Enzyme mechanism. A** | CV of *A. aeolicus* NiFe hydrogenase adsorbed on a graphite electrode.  
1365 Electrode rotation rate 4000 rpm, scan rate  $0.3 \text{ mV s}^{-1}$ , pH 7, 40 °C, 1 atm. H<sub>2</sub>. Arrows indicate the  
1366 direction of the sweeps. **B** | CA of *A. aeolicus* NiFe hydrogenase. Electrode rotation rate 4000 rpm, pH  
1367 8, 40 °C, 1 atm. H<sub>2</sub>. WE potential against time (upper panel). Catalytic current (red) against time and  
1368 fit (green) (lower panel). Film loss during measurement accounts for the lower H<sub>2</sub> oxidation current at  
1369 approx. 500 s that at  $t = 0$ . **C** | Structure of *D. fructosovorans* NiFe hydrogenase (upper). Detail of the  
1370 gas tunnel leading to the active site in wild type enzyme (lower left) and the I74, F122 variant (lower  
1371 right). **D** | CA of *D. fructosovorans* NiFe hydrogenase wild-type enzyme (left) and the L122F-V74I  
1372 mutant (right) under 1 atmos. H<sub>2</sub> and exposed to carbon monoxide (CO) at  $t = 0$ . Enzyme adsorbed on  
1373 a PGE WE. Electrode rotation rate 2000 rpm.

1374



1376

1377 **Glossary**

1378 Chronoamperometry a technique in which electric current is measured as a function of time with the  
1379 WE held at a defined electric potential, or stepped between two or more defined electric potentials.

1380 Counter electrode – an electrode that carries electric current flowing in a three-electrode  
1381 electrochemical cell. Electrochemical processes occurring at this electrode are not of interest.

1382 Cyclic voltammetry – a technique in which the current is measured as the WE potential is ramped  
1383 linearly with time. When a defined WE potential is reached, the potential is ramped linearly in the  
1384 opposite direction to return the WE to its initial potential.

1385 Faradaic current – electric current generated by the oxidation or reduction of species at a WE.

1386 Non-Faradaic current – electric current measured in an electrochemical cell that is not due to redox  
1387 processes. Typically, this current arises from migration of ions in response to the electric potential  
1388 applied to an electrode.

1389 Redox catalysis - the interconversion of reactants and products through a redox reaction catalysed  
1390 by an enzyme. For an enzyme catalysed reaction the reactants are often referred to as substrates.

1391 Reference electrode – an electrode with a stable and defined electrode potential. The potential of  
1392 the working electrode is defined relative to that of the reference electrode.

1393 Working electrode – the electrode at which redox chemistry of interest occurs in a three-electrode  
1394 electrochemical cell.